Triple Evolution Pathways to Black Hole Low-Mass X-ray Binaries: Insights from V404 Cygni

Cheyanne Shariat ,[1, 2, 3] Smadar Naoz ,[2, 3] Kareem El-Badry ,[1] Kyle Akira Rocha ,[4, 5]
Vicky Kalogera ,[4, 5] Alexander P. Stephan ,[6] Kevin B. Burdge ,[7, 8] and Isabel Angelo [2, 3]

[1] Department of Astronomy, California Institute of Technology, 1200 East California Boulevard, Pasadena, CA 91125, USA
[2] Department of Physics and Astronomy, University of California, Los Angeles, Los Angeles, CA 90095, USA
[3] Mani L. Bhaumik Institute for Theoretical Physics, University of California, Los Angeles, Los Angeles, CA 90095, USA
[4] Department of Physics & Astronomy, Northwestern University, 2145 Sheridan Road, Evanston, IL 60208, USA
[5] Center for Interdisciplinary Exploration and Research in Astrophysics (CIERA), 1800 Sherman, Evanston, IL 60201, USA
[6] Department of Physics and Astronomy, Vanderbilt University, 1221 Stevenson Center Lane, Nashville, TN 37240, USA
[7] Department of Physics, Massachusetts Institute of Technology, Cambridge, MA 02139, USA
[8] Kavli Institute for Astrophysics and Space Research, Massachusetts Institute of Technology, 7 Cambridge, MA 02139, USA

ABSTRACT

A recent discovery shows that V404 Cygni, a prototypical black hole low-mass X-ray binary (BH-LMXB) is a hierarchical triple: the BH and donor star are orbited by a 1.2 $M_\odot$ tertiary at a distance of at least 3500 au. Motivated by this system, we evolve a grid of $\sim 50,000$ triple star systems, spanning a broad range of initial orbits. Our calculations employ `MESA` stellar evolution models, using `POSYDON`, and self-consistently track the effects of eccentric Kozai-Lidov (EKL) oscillations, mass loss, tides, and BH natal kicks. In our simulations, the progenitors of V404 Cygni-like systems have initial outer separations of $1000 - 10000$ au and inner separations of ~ 100 au, such that they avoid Roche lobe overflow most of the time. Later on, EKL oscillations drive the inner binary to high eccentricities until tides shrink the orbit and mass transfer begins. Notably, such systems only form in simulations with very weak black hole natal kicks ($\lesssim 5\,\mathrm{km\,s^{-1}}$) because stronger kicks unbind the tertiaries. Our simulations also predict a population of BH-LMXB triples that form via the classical common-envelope channel, when the BH progenitor does overflow its Roche lobe. The formation rate for this channel is also higher in triples than in isolated binaries because early EKL oscillations cause inner binaries with a wider range of initial separations to enter and survive a common envelope. Our calculations demonstrate that at least some stellar BHs form with extremely weak kicks, and that triple evolution is a significant formation channel for BH-LMXBs.

1. INTRODUCTION

Black Hole low-mass X-ray Binaries (BH-LMXBs) are binary star systems where a black hole (BH) accretes material from a low-mass stellar companion ($\lesssim$ 1-2 $M_\odot$). The companions are usually main-sequence (MS), subgiant, or giant stars, and their mass transfer creates an accretion disk around the BH (Shakura 1973), producing X-ray emission. Currently, about 25 BH X-ray binary systems have been dynamically confirmed in the Galaxy, most of which are BH-LMXBs (Corral-Santana et al. 2016). BH-LMXBs mostly reside in quiescent states, characterized by an X-ray luminosity below $\sim 10^{32}$ erg s^{-1}, but can exhibit outbursts with X-ray luminosities reaching up to $\sim 10^{39}$ erg s^{-1} for sources accreting near the Eddington limit (see, e.g., Bahramian &

Degenaar 2023, for a review). BH-LMXBs are widely associated with old stellar populations such as the Galactic center, Galactic bulge, and Galactic clusters (e.g., Arnason et al. 2021; Bahramian & Degenaar 2023). About half of the known BH-LMXBs are in the Galactic disk (van Paradijs & White 1995; White & van Paradijs 1996; Grimm et al. 2002; Tetarenko et al. 2016; Bahramian & Degenaar 2023, see figure 9 of the latter for a complete summary). Large galactic latitudes are more common among neutron star-LMXBs, likely indicating that they were born with higher kicks (Fragos et al. 2009; Repetto et al. 2012, 2017; Atri et al. 2019; Wong et al. 2014; Kimball et al. 2023).

Stellar black holes, including those in BH-LMXBs, are thought to be the remnants of massive progenitor stars ($\gtrsim 20 - 40 M_\odot$, e.g., Fryer et al. 2012). Most stars of this mass do not evolve in isolation and instead have one or more stellar companions (e.g., Sana et al. 2012; Kobulnicky et al. 2014; Moe & Di Stefano 2017; Offner

et al. 2023). Stellar BH progenitors are theorized to have initial radii above ~ 10 R$_\odot$, which expand and become significantly larger during the post-main sequence evolution ($\sim 1000 - 3000$ R$_\odot$, e.g., Levesque et al. 2005; Romagnolo et al. 2023). During this expansion, any companion within ~ 10 au would likely interact with the primary before it becomes a BH. If the companion's mass is low, as is the case in LMXBs, common envelope (CE) evolution is expected to commence (e.g., Ivanova et al. 2020), where the low-mass secondary is engulfed in the extended envelope of the BH primary (e.g., Kalogera & Webbink 1996, 1998; Kalogera 1999a; Tauris & van den Heuvel 2006a; Taam & Ricker 2010; Ivanova et al. 2013).

One potential challenge in forming BH-LMXBs through the aforementioned isolated binary evolution channel lies in the common envelope stage. Specifically, considering the energy budget of the system, a low-mass star may not have sufficient orbital energy to unbind the envelope of the black hole progenitor during the unstable CE stage (e.g., Portegies Zwart et al. 1997; Kalogera 1999b; Podsiadlowski et al. 2003; Justham et al. 2006). To resolve this challenge, several ideas were suggested, involving additional sources of energy during the CE phase to successfully eject the envelope (e.g., Podsiadlowski et al. 2010; Ivanova 2011; Ivanova et al. 2015). Specifically, it was suggested by Ivanova (2011) that the enthalpy of the envelope should be included in the energy budget calculation, which leads to an overall lowering of the binding energy of the envelope. Recent binary stellar evolution studies demonstrated that this channel could then lead to the formation of LMXBs, such as IC 10 X-1 and MAXI J1305-704 (e.g., Wong et al. 2014; Kimball et al. 2023). Another energy source that may help eject the envelope is nuclear energy sources in the shocked-induced detonation wave that may disrupt the surrounding gas (e.g., Ivanova et al. 2002; Podsiadlowski et al. 2010). Another set of ideas presented in the literature focused on the companion itself. For example, it was suggested that the low-mass companion formed from the disrupted envelope of the massive primary (e.g., Podsiadlowski et al. 1995), or that the companion was initially a larger star and low-mass star observed today is a result of the mass transfer process (e.g., Podsiadlowski & Rappaport 2000; Chen et al. 2006; Justham et al. 2006). Another set of models relies on dynamically assembling the companion after the BH formed (e.g., Clark & Parkinson 1975; Hills 1976; Voss & Gilfanov 2007; Giesler et al. 2018; Kremer et al. 2018).

One mechanism that can produce BH-LMXBs without early mass transfer is through three-body dynamics (e.g., Eggleton & Verbunt 1986; Michaely & Perets 2016; Naoz et al. 2016). A significant fraction of massive stars are born in triple and higher order systems ($68 \pm 18\%$, e.g., Sana et al. 2012, 2014; Moe & Di Stefano 2017; Offner et al. 2023). From birth, triple star systems remain stable by naturally tending towards hierarchical configurations (Duchêne et al. 2013): two stars orbit closely (the inner binary) relative to the tertiary star's wider orbit about the inner binary (the outer binary, see Figure 1). In hierarchical triples, the inner binary can begin wide enough, avoiding the CE prior to BH formation. Once the primary undergoes core collapse, the binary will then become a detached BH+low-mass main-sequence binary with a separation of $10 - 1000$ au. At this point, the tertiary can tighten this inner binary through the combined effects of the eccentric Kozai-Lidov Mechanism (EKL), stellar evolution, and tidal capture (e.g., Kozai 1962; Lidov 1962; Fabrycky & Tremaine 2007; Naoz 2016; Naoz et al. 2016; Stephan et al. 2016, 2019; Toonen et al. 2016; Shariat et al. 2023, 2024; Weldon et al. 2024). Secular EKL oscillations from the tertiary can cause extreme eccentricities in the binary that would decrease the periastron of the orbit to less than $10 - 100$ solar radii (e.g., Naoz et al. 2016). At such close periastron distances, tides, magnetic braking, and mass transfer can dissipate orbital energy and angular momentum to shrink the orbit on relatively short timescales, forming a BH-LMXB. Any post-MS stellar evolution of the secondary star increases the probability of earlier tidal locking or mass transfer, making the triple channel even more efficient. This three-body formation scenario has been studied for producing LMXBs in Naoz et al. (2016), as well as other accreting compact objects (Toonen et al. 2016; Stephan et al. 2019; Shariat et al. 2023, 2024).

One process that may inhibit the triple formation scenario is the presence of a BH natal kick. From stability arguments, the tertiary of a wide BH binary must be at least $5 - 10$ times further from the inner binary than the separation of the inner binary (e.g., Mardling & Aarseth 2001). This means that typical tertiary distances in BH triples are $500 - 10^4$ au (Naoz et al. 2016). At these distances, the tertiary is so weakly bound that even a small kick would unbind the orbit in most cases. The prevalence and typical magnitude of BH natal kicks are uncertain. Theoretical studies have proposed mechanisms where BHs can form through nearly complete implosions with negligible kicks (e.g., Woosley & Weaver 1995; Sukhbold et al. 2016; Mirabel 2017) Studies of different BH X-ray binaries have derived a wide range of natal kick velocities for different systems. In general, many studies out kick velocities greater than 80-100 km s^{-1} (e.g., Mandel 2016) and often support small (to null)

natal kicks (e.g., Reid et al. 2014; Mirabel 2017; Shenar et al. 2022), with the exception of some systems, such as XTE J1118+40 and MAXI J1305-704, (e.g., Fragos et al. 2009; Andrews & Kalogera 2022; Dashwood Brown et al. 2024; Kimball et al. 2023).

Recently, Burdge et al. (2024) discovered that V404 Cygni is orbited by a wide tertiary at 3500 au separation, making V404 Cygni part of a hierarchical triple system (see Figure 1 for a schematic). While the possibility of the existence of tertiary companions was suggested in the past for other systems, (e.g., Grindlay et al. 1988; Corbet et al. 1994; Thorsett et al. 1999; Chou & Grindlay 2001; Prodan & Murray 2015; Dage et al. 2024), V404 Cygni is the first robust detection of a BH-LMXB with a wide tertiary companion. At a distance of 2.4 kpc, the system contains a ~ 9 $M_\odot$ BH (Khargharia et al. 2010) accreting from a 0.7 $M_\odot$ evolved companion with radius $R \sim 6\,R_\odot$ (Shahbaz et al. 1994) at a separation of 0.14 au ($P_{\rm orb} = 6.4$ days). This makes it one of the widest known BH-LMXBs (e.g., Corral-Santana et al. 2016). Additionally, spectral fitting of the tertiary showed that it is beginning to evolve off of the main sequence and is currently at twice its initial radius (Burdge et al. 2024). Through isochrone analysis, Burdge et al. (2024) constrain the mass of the tertiary to ~ 1.2 $M_\odot$ and the system's age to $3 - 5$ billion years. The fact that the K-giant companion in the V404 LMXB is more evolved than the tertiary indicates that the inner companion was initially more massive than 1.2 $M_\odot$, or equivalently, has since lost at least 0.5 $M_\odot$ through accretion onto the BH.

Here, we investigate the evolutionary history of V404 Cygni and the broader population of BH-LMXBs with wide companions. We specifically test formation pathways and the impact BH natal kicks have in such systems and compare them to isolated binary formation models. In Section 2 we outline the three-body simulations. In Section 3, we discuss the results from the simulations and their implications for BH natal kicks. We also compare our isolated binary models to the triples to predict the likely formation of Galactic BH-LMXBs. In Section 4, we discuss the time of LMXB formation and how it can potentially distinguish different formation pathways. In Section 5, we provide a prediction for the outer tertiary's orientation, in Section 7 and Section 6 we itemize and discuss our main conclusions, respectively.

2. METHODOLOGY

2.1. *Simulations*

2.1.1. *Three-Body Dynamics*

Throughout this study, we consider a hierarchical triple system with masses m_1, m_2, in the inner binary, and m_3 on a wider orbit about the inner binary (the tertiary). The triple has an inner (outer) semi-major axis a_1 (a_2), eccentricity e_1 (e_2), argument of periapsis ω_1 (ω_2), and inclination with respect to the total angular momentum vector i_1 (i_2). See Figure 1 for a schematic representation of such a hierarchical triple.

In our simulations, we solve the hierarchical three-body equations of motion up to the octupole level of approximation (see Naoz 2016, for the full set of equations). We also include the effects of general relativistic precession for both the inner and outer orbit to 1st post-Newtonian order (e.g., Naoz et al. 2013b). In the mass ratios studied here, the first-order description is sufficient to model the dynamics (e.g., Naoz et al. 2013b; Lim & Rodriguez 2020; Kuntz 2022). For the inner binary, we also model the tidal effects by adopting the equilibrium tides model (Hut 1980; Eggleton et al. 1998; Kiseleva et al. 1998; Naoz 2016, see the latter for the full set of the equations in their appendix B). This prescription includes tidal precession, rotational precession, and tidal dissipation, the latter of which is modeled assuming a viscous time of 5 yr (following, e.g., Naoz & Fabrycky 2014; Naoz et al. 2016; Stephan et al. 2016). Using our tidal model, we can follow the spin precession of stars in the inner binary, which arise from tidal torques and oblateness (e.g., Naoz & Fabrycky 2014). The tidal models for main-sequence (MS) stars are convective, while those of red-giant (RG) stars are radiative (e.g., Zahn 1977). The switch between tidal models takes place as a function of stellar type and mass (see Rose et al. 2019; Stephan et al. 2018, 2019, 2021). For white dwarfs (WDs), neutron stars (NSs), and black holes (BHs), equilibrium tides are assumed. Magnetic braking is modeled with the stellar evolution part of the code (see below) following Rappaport et al. (1983).

2.1.2. POSYDON *Single Stellar Evolution*

In hierarchical triples, the changes in stellar masses and radii associated with stellar evolution can impact the evolution of the system by re-triggering or suppressing EKL (e.g., Naoz 2016; Stephan et al. 2016), expanding the inner orbit's semi-major axis faster than that of the outer binary (e.g., Perets & Kratter 2012; Shappee & Thompson 2013; Michaely & Perets 2014; Naoz 2016), circularizing the inner binary via tidal interactions (e.g., Liu et al. 2015; Bataille et al. 2018; Angelo et al. 2022), leading to mass transfer (e.g., Salas et al. 2019; Toonen et al. 2020; Shariat et al. 2023), or even causing a complete stellar merger (e.g., Antonini et al. 2016; Toonen et al. 2018; Stephan et al. 2016, 2019; Shariat
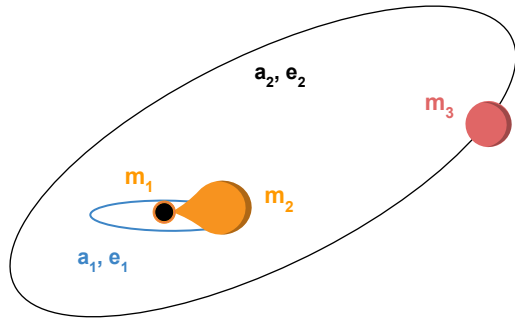
Figure 1. Schematic of V404 Cygni in a hierarchical triple. The triple system contains a close 'inner binary' with a semi-major axis and eccentricity of a_1 and e_1, respectively. The distant tertiary orbits the inner binary, creating the 'outer binary', which has a respective semi-major axis and eccentricity of a_2 and e_2. In the inner binary, a $m_1 = 9$ M$_\odot$ black hole accretes from a $m_2 = 0.7$ M$_\odot$ evolved companion in a circular orbit with $a_1 \sim 0.1$ au, classifying it as a low-mass X-ray binary. At a separation of 3500 au away, $m_3 = 1.2$ M$_\odot$ orbits the inner binary, which is also an evolved star. Based on the evolved tertiary, the system's age is 4 ± 1 Gyr. This layout is widely similar for all BH-LMXBs with wide companions.

et al. 2024). However, nearly all previous studies that examine stellar evolution in a triple framework use the rapid fitting formulae of `Single Stellar Evolution` (`SSE`, Hurley et al. 2000; Hurley et al. 2002), or a variation thereof. The evolution of the component stars can be more accurately followed using detailed stellar models such as MESA (Paxton et al. 2011). However, these codes are not often employed for running a large number of simulations because they are slower and more computationally expensive than rapid binary population synthesis codes (e.g., Paxton et al. 2019; Hurley et al. 2000).

Recently, Fragos et al. (2023) developed `POSYDON`: POpulation SYnthesis with Detailed binary-evolution simulatiONs. `POSYDON` is a general-purpose code that is capable of evolving a population of binaries on a framework that uses self-consistent stellar evolution models. `POSYDON` adopts detailed single binary evolution tracks computed with the Modules for Experiments in Stellar Astrophysics (`MESA`; Paxton et al. 2011, 2013, 2015, 2018, 2019; Jermyn et al. 2023). In this analysis, we use `MESA` single-star tracks and interpolation routines distributed with `POSYDON v1` to follow the evolution of the component stars. Single-star `MESA` models self-consistently model the star's structural response to mass-loss through winds, leading to significant deviations in stellar properties (e.g., final masses and radii) compared to SSE (Fragos et al. 2023).

To perform single stellar evolution in `POSYDON`, we place a single star into a non-interacting binary and only focus on the evolution of the primary star of interest. Specifically, we place our primary star of interest (with given initial mass, metallicity, and spin) into a wide ($a > 10^5$ au) circular binary with a 0.5 M$_\odot$ secondary star. This configuration, a wide orbit with a low-mass secondary, eliminates any chance of the secondary affecting the properties of the primary and is effectively just a single stellar evolution of the primary. Next, we generate a time series of the parameters for the primary for a given evolution time (often 10 Gyr here). `POSYDON v1` evolve each star in a detached binary using MESA grids, making our method of single star evolution equivalent to interpolating on single-star `MESA` tracks, with a parameterized CO core mass to compact object mass relation.

`POSYDON` includes several subgrid prescriptions for predicting compact object mass (BH or NS) based on the properties of the progenitor before core collapse. Note that although the different prescriptions share many similarities, they have noticeable differences in the final compact object masses near the NS/BH progenitor mass boundary. Specifically, we use two models. The first is the default core-collapse model from Patton & Sukhbold (2020), which utilizes the average carbon abundance at carbon ignition to determine the explodability of the core and assumes that BHs form only from a failed explosion in direct collapse. In this scenario, a ~ 21 M$_\odot$ progenitor star collapses into a ~ 9 M$_\odot$ BH. The second core-collapse model we utilize is the Fryer et al. (2012) *delayed*. In this channel, a ~ 28 M$_\odot$ progenitor star collapses into a ~ 9 M$_\odot$ BH. For the BH masses considered here, the two models gave consistent outcomes.

We determine the secondary's stellar type during its evolution by assessing the radius of the star. All of the secondary stars in the inner binary began with $R_2 = 1 - 1.5$ R$_\odot$, so we consider an 'RG' to be any evolved star with $R_2 > 2.0$ R$_\odot$, though most have much radii much larger than this cutoff. Secondary stars with $R_2 < 0.02$ R$_\odot$ are considered white dwarfs, and the rest are considered to be on the main sequence.

Most previous studies of triples used `SSE` or `BSE` (Hurley et al. 2000, 2002), which can radically alter the evolution of a binary or triple relative to `POSYDON`. One notable difference is that the wind prescriptions in SSE are highly optimistic, and likely outdated (Hurley et al. 2000; Paxton et al. 2015). For example, a 22 M$_\odot$ zero-age main-sequence (ZAMS) star in SSE expands to almost 7 au during its red supergiant phase, which is nearly 3 au greater than predicted from `POSYDON`, or equivalently `MESA`, at solar metallicity. Though these

models are likely more consistent than SSE, they are still uncertain (Romagnolo et al. 2023). ZAMS stars also evolve more quickly in SSE, making it difficult to compare timescales or ages from simulations to observed stellar populations. Furthermore, in our analysis, we notice that the supergiant phase lasts longer in SSE, and the mass loss associated with it occurs in many discrete steps over the course of Myrs. If the star is embedded in a hierarchical triple, this evolution alters the dynamics and subsequent evolution of the entire triple on these timescales and creates a larger probability of tidal locking. Each discrete mass loss episode changes the mass ratios in the triple, which thereby changes the dynamics during these periods. We touch on this difference more in Section 2.4. Three-body evolution is generally less sensitive to uncertainties in stellar evolution when the stars are not transferring mass before BH formation. All of the results that follow in this work leverage single-star modeling from MESA to evolve all three stars in the hierarchical triples.

2.1.3. *Formation Kicks*

Another new addition to our triple code is the consideration of kicks (with kick velocity v_k), including natal kicks during WD, NS, and BH formation. In general, kicks can tilt orbits, change their eccentricities, or unbind them completely. Neutron stars are inferred to experience natal kicks on the order of 100s of km s^{-1} (e.g., Lyne & Lorimer 1994; Hansen & Phinney 1997; Lorimer et al. 1997; Cordes & Chernoff 1998; Fryer et al. 1999; Hobbs et al. 2004). These kicks are essential to the evolution of NSs with companions as they can account for the spin misalignment in pulsar binaries (Lai et al. 1995; Kalogera 1996; Kaspi et al. 1996; Kalogera 2000), hypervelocity neutron stars (Fragione et al. 2017; Fragione & Loeb 2017; Lu & Naoz 2019; Zubovas et al. 2013; Hoang et al. 2022; Jurado et al. 2024), and perhaps also the eccentricity of wide NS binaries (El-Badry et al. 2024a,b) for weaker kicks. Kicks are also expected to exist during WD formation due to asymmetric mass loss on the AGB, following El-Badry & Rix (2018); Shariat et al. (2023, 2024); Stephan et al. (2024).

Lastly, when kicks are selected in the simulations, we consider the effects of BH natal kicks. Currently, the magnitude of BH natal kicks and their frequency is uncertain. Most estimates are made by combining observed spatial velocities with binary evolution models to constrain kick magnitudes in BH X-ray binaries (e.g., Mirabel et al. 2001; Mirabel & Rodrigues 2003; Jonker & Nelemans 2004; Willems et al. 2005; Fragos et al. 2009; Repetto et al. 2012; Wong et al. 2014; Repetto & Nelemans 2015; Repetto et al. 2017; Mandel 2016).

However, these estimates are often model-dependent, sometimes conflict with one another, and can be accompanied by large uncertainties. For example, some studies conclude that some BHs form with relatively high kicks, $v_k \gtrsim 80 - 100$ km s^{-1} (Fragos et al. 2009; Repetto et al. 2012; Repetto & Nelemans 2015; Repetto et al. 2017; Mandel 2016; Beer & Podsiadlowski 2002; Kimball et al. 2023; Mata Sanchez et al. 2024). The BH-LMXB V404 Cygni was initially inferred to have experienced a ~ 65 km s^{-1} BH natal kick (Miller-Jones et al. 2009), though this is unlikely to be true given the observed wide companion's presence. For example, it was estimated that XTE J1118+480 had a natal kick of $v_k \gtrsim 80$ km s^{-1} (Fragos et al. 2009). Additionally, another system observed via astrometric microlensing, MOA-2011-BLG-191/OGLE-2011-BLG-0462, placed an upper limit of $v_k \lesssim 100$ km s^{-1} (Andrews & Kalogera 2022). The recently dynamically confirmed BH-LMXB, Swift J1727.8-1613, was also estimated to form with $v_k > 200$ km s^{-1}, based on its spatial velocity (Mata Sanchez et al. 2024). Similarly, large space velocities were observed in MAXI J1305-704, leading to a constraint of $\gtrsim 70$ km s^{-1} on the BH natal kick magnitude. It is also possible that large spatial velocities are the result of dynamical heating from neighboring perturbers, especially for BH-LMXBs, which are generally old (Zhang et al. 2012; van Paradijs & White 1995). Some of these systems may have also formed in stellar clusters, where various dynamical processes can cause runaway velocities (e.g., Poveda et al. 1967; Rodriguez et al. 2015).

On the other hand, several observations rule out the presence of any significant BH natal kicks. Recently, V404 Cygni, a BH-LMXB with a wide tertiary, was reported to have formed with nearly no kick $v_k < 5$ km s^{-1}, on the basis of its bound tertiary in a wide orbit (Burdge et al. 2024). Furthermore, for the massive X-ray-faint binary, VFTS 243, a low observed eccentricity suggests that the BH received a negligible natal kick if any (Shenar et al. 2022; Vigna-Gómez et al. 2024). Studies of Cygnus X-1, a BH X-ray source, show that it likely formed in situ, with a negligible kick (Mirabel & Rodrigues 2003). Other studies have also suggested small ($0 - 80$ km s^{-1}) BH natal kicks (Reid et al. 2014; Wong et al. 2012; Mirabel 2017). For a detailed discussion of the broader landscape of BH natal kicks, see Mirabel (2017). In this study, we test whether BH-LMXBs in hierarchical triples experience BH formation kicks.

When kicks are activated in our models, every compact object formation triggers an added kick velocity to the newly born compact remnant. The kick velocity for

any type of compact object (WD, NS, or BH) is sampled from the Maxwell-Boltzmann distribution:

$$f(v_k) = \sqrt{\frac{2}{\pi}} \frac{v_k^2}{\sigma^3} \exp\left(\frac{-v_k^2}{2\sigma^2}\right) . \qquad (1)$$

For NS kicks, the median value of v_k is 400 km s^{-1} with a standard deviation of $\sigma = 265$ km s^{-1} (Hansen & Phinney 1997; Arzoumanian et al. 2002; Hobbs et al. 2004), though our triple do not produce an NSs. For BHs, we sample from the NS distribution but scale the kick velocity by 1.4 M$_\odot$/M_{BH}, where M_{BH} is the gravitational mass of the BH in solar masses. This effectively assumes that BH and NS kicks have the same linear momentum. For WDs v_k is chosen from the same Maxwellian in Equation 1 but with median value $v_k = 0.75$ km s^{-1} and $\sigma = 0.5$ km s^{-1} (El-Badry et al. 2018). Since the resulting orbital parameters are dependent on the orbital orientation of the binary before the kick and on the direction of the kick (e.g., Lu & Naoz 2019), we randomize both of these at the time of the kick. The post-kick orbital parameters are calculated analytically following Lu & Naoz (2019)[1], whose prescriptions also determine whether the inner and outer orbit remain bound.

2.2. Numerical Setup

For all of our models, we fix the initial mass of the tertiary to $m_3 = 1.2$ M$_\odot$, based on observations (Burdge et al. 2024). Since the secondary is observed to be more evolved than the tertiary, m_2 was likely greater than m_3 initially (Burdge et al. 2024). Following this observation, we sample the secondary mass from a uniform distribution ranging from $1.2 - 2.0$ M$_\odot$. A 2.0 M$_\odot$ would evolve in ~ 1 Gyr, which is 2 standard deviations below the constrained age, so we choose it as the upper mass limit. Today, V404 Cygni has a black hole with $m_1 = 9^{+0.2}_{-0.6}$ M$_\odot$ (Khargharia et al. 2010). Therefore, we choose an m_1 zero-age main-sequence (ZAMS) mass based on the supernova prescription used in POSYDON for our particular model. In the models where the SN_STEP engine is the Patton & Sukhbold (2020) core collapse model, we assume an $m_1 = 21.7$ M$_\odot$ initially, which leads to a ~ 9.2 M$_\odot$ BH. In the models where we choose the SN_STEP engine to be the Fryer et al. (2012) *delayed* core collapse model, we choose an $m_1 = 27$ M$_\odot$ initially, which also leads to a ~ 9.2 M$_\odot$ BH. Testing different core-collapse prescriptions is effectively testing how different amounts of mass loss affect the final orbital structure. However, preliminary results showed a

---

[1] see also Hamers et al. (2018); Hoang et al. (2022); Jurado et al. (2024)

minimal difference between the models with different SN prescriptions.

For all of our models, we sample the inner/outer periods from a log-uniform distribution between $0.1 - 10^4$ years. We draw the inner/outer eccentricities from a uniform distribution and draw the inner/outer inclinations from an isotropic distribution (uniform in $\cos i$). The initial spin-orbit angles are also drawn uniformly. After sampling initial conditions for the triple, we require that these parameters satisfy long-term and dynamical stability criteria. The first criterion simply requires that the triple is hierarchical. To test hierarchy, we adopt the hierarchical criterion ϵ, which describes the pre-factor of the octupole level of approximation (e.g., Naoz et al. 2013a)

$$\epsilon = \frac{a_1}{a_2} \frac{e_2}{1 - e_2^2} < 0.1 . \qquad (2)$$

To enforce long-term stability, we apply the criteria from Mardling & Aarseth (2001):

$$\frac{a_2}{a_1} > 2.8 \left(1 + \frac{m_3}{m_1 + m_2}\right)^{\frac{2}{5}} \frac{(1 + e_2)^{\frac{2}{5}}}{(1 - e_2)^{\frac{6}{5}}} \left(1 - \frac{0.3i}{180°}\right) . \qquad (3)$$

Deviation from a complete hierarchy does not necessarily mean an instantaneous breakup of the system or an immediate instability (Grishin et al. 2017; Mushkin & Katz 2020; Bhaskar et al. 2021; Toonen et al. 2022; Zhang et al. 2023). However, since V404 Cygni is in a hierarchical triple configuration today, we take the conservative approach and require only stable, hierarchical systems based on the aforementioned criteria.

We run each triple simulation for an upper limit of 10 Gyr, but systems are stopped earlier if the inner binary (1) crosses the Roche limit or (2) becomes unbound due to kicks. The latter condition is calculated analytically following Lu & Naoz (2019) for the simulations that included kicks. For the first condition, we require that $a_1(1 - e_1) > R_{Roche}$ so that there is no immediate Roche crossing in the inner binary. Here, the Roche limit, R_{Roche}, is defined by

$$R_{Roche,ij} = \frac{R_j}{\mu_{Roche,ji}} , \qquad (4)$$

where $j \in 1, 2$ represents the two stars in the inner binary and R_j is the radius of the star with mass m_j. $\mu_{Roche,ji}$ is the approximate Roche radius given by (Eggleton 1983)

$$\mu_{Roche,ji} = \frac{0.49(m_j/m_i)^{2/3}}{0.6(m_j/m_i)^{2/3} + \ln(1 + (m_j/m_i)^{1/3})} \qquad (5)$$

To determine whether the inner binary of a triple system became an LMXB, we filter for systems that meet these criteria:

Table 1. Simulations Statistics

	Model 1	Model 2	Model 3	Model 4	Model 5
Kicks	No	Yes	No	No	Yes
Periods	DM91	DM91	LU	LU	LU
SN_STEP	PS20	PS20	F12d	PS20	F12d
N_{Total}	2101	795	839	15594	962
N_{Roche}	1576	688	734	13719	833
N_{BH}	525	107	301	2964	129
N_{LMXB}	48	4	8	375	13
$N_{\text{V404 Cygni}}$	14	1	5	102	6

Description of the different simulations used in this study. The 'Kicks' row specifies whether supernova and WD kicks were assumed. The 'Periods' row specifies the initial period distribution that was used. Here, 'LU' refers to log-uniform, and DM91 is a reference to the period distribution in Duquennoy & Mayor (1991). The 'SN_STEP' row specifies the supernova engine used: i.e., the mapping between progenitor properties and BH mass. Here, PS20 refers to Patton & Sukhbold (2020) and F12d is in reference to the *delayed* core-collapse model from Fryer et al. (2012). N_{Total} gives the total number of simulations run for each model. N_{Roche} gives the number of inner binaries that experienced Roche Lobe Overflow with the BH progenitor, i.e., before the BH formed, according to POSYDON. N_{BH}, N_{LMXB}, and $N_{\text{V404 Cygni}}$ respectively are the number of systems that formed a black hole in the inner binary without a mass transfer with the BH progenitor, the number that became LMXBs, and the number of LMXBs that had orbital configuration similar to V404 Cygni.

1. The primary star in the inner binary is a BH.

2. The pericenter of the inner binary is within two times the Roche radius of the secondary star (e.g., Fabian et al. 1975).

3. The secondary star is on the main sequence or giant branch.

In Table 1, we summarize the different models we used along with their relevant population statistics. While we initially considered various supernova models, most of the statistical analysis (Section 3.4) focus on those with a log uniform (LU) initial period distribution and a 'PS20' core collapse prescription from (Patton & Sukhbold 2020) for consistency.

2.3. *Post-Roche Lobe Crossing Tidal Evolution*

Once the star crosses its Roche Lobe (RL), we expect the inner binary to decouple from the tertiary. We in-

tegrate all of these systems forward using our tidal prescription. At this stage we numerically integrate the a_1 and e_1 evolution (similar to Angelo et al. 2022) using the coupled tidal equations (Eggleton & Kiseleva-Eggleton 2001):

$$\frac{a}{|\dot{a}|} = \frac{t_v f_T(e_1)}{162(1+2k_s)^2} \frac{m_2^2}{m_1(m_1+m_2)} \left(\frac{a_1}{R_2}\right)^8 \times \frac{(1-e_1^2)^{15/2}}{e_1^2}, \tag{6}$$

$$\frac{e}{|\dot{e}|} = \frac{t_v f_T(e_1)}{81(1+2k_s)^2} \frac{m_2^2}{m_1(m_1+m_2)} \left(\frac{a_1}{R_2}\right)^8 \times (1-e_1^2)^{13/2}. \tag{7}$$

Here, R_2 is the radius of the secondary, a_1 is the inner orbit's semi-major axis, e_1 is the inner orbit's eccentricity, m_1 is the mass of the primary (in our case, the black hole), m_2 is the mass of the secondary, t_v is viscous timescale (as mentioned, set to 5 yr in our simulations), k_s is the classical apsidal motion constant (set to 0.25), and $f_T(e_1) \equiv 1 + \frac{3}{2}e_1^2 + \frac{1}{8}e_1^4$. Our choice of k_s corresponds to a tidal quality factor of $Q \approx 1.8 \times 10^6$ (see Eggleton & Kiseleva-Eggleton 2001; Naoz 2016). Recall that in the dynamical simulations, we use the complete formalism of Eggleton & Kiseleva-Eggleton (2001), which considers spin rates of both stellar components as well (Naoz 2016). Importantly, Equation (6) is the tidal shrinking timescale $t_{shrink} = a/|\dot{a}|$, and Equation 7 is the tidal circularization timescale $t_{circ} = e/|\dot{e}|$. If $a_1 = 1000$ au, $e_1 = 0.999$, $m_1 = 9$ M$_\odot$, $m_2 = 1$ M$_\odot$, $R_2 = 1$ R$_\odot$, then $t_{shrink} \sim 1$ yr and $t_{circ} \sim 1000$ yr. These chosen orbital parameters are characteristic of a typical triple in EKL-induced tidal descent and show that tidal forces act on timescales that are generally much quicker than stellar evolution timescales.

Using the Equation (6) and (7), we numerically integrate the triples that are halted in the simulations during this phase. We integrate these systems up to $t = 5$ Gyr to match the upper constraint on the age of V404 Cygni (Burdge et al. 2024) and show the results in Figure 2. Note these timescales evolve nonlinearly in time, as the shorter, shrinking timescale shortens the orbit, allowing for a more rapid circularization. In many cases, tides shrink and circularize the orbits in less than a Gyr. The top row of Figure 2 shows the parameters are the last timestep of the simulations, and the bottom panels include the results of tidal evolution post-RL crossing. In the first column, we color the systems by the stellar type of the secondary. Overall, the smaller, main-sequence secondaries (green points) require shorter pericenter distances to initiate mass transfer or efficient tidal dissipation. On the other hand, the larger red giant
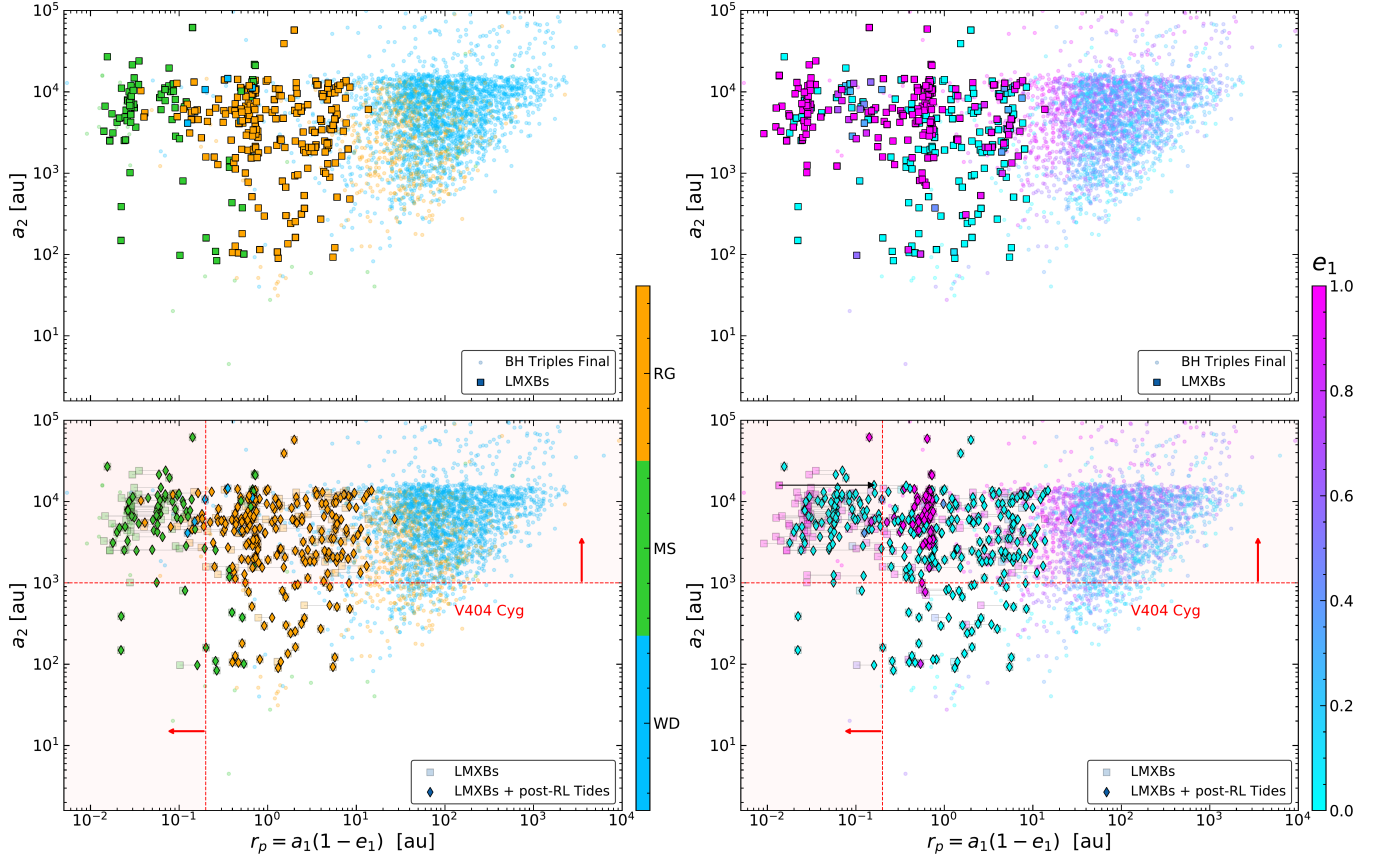
Figure 2. Effect of tides on the periastron of interacting binaries. The top row shows the outer semi-major axis, a_2, as a function of the periastron distance at the last step of the simulations. Square points denote triples with inner BH-LMXBs, and all circular points are detached BH binaries. The bottom row is the same as the top but shows the parameters after tidal evolution. The left and right columns present the same data; only the left is colored by stellar type, and the right is colored by eccentricity. Here, we took all of the LMXBs from the top panel (squares) and evolved their orbits post Roche Lobe crossing as described in Section 2.3. The post-tides parameters are plotted with diamonds, and a gray line connects the pre-tides to the post-tidal evolution parameters. Tides generally serve to circularize the orbit faster than it is shrunk, resulting in slightly larger periastron distances overall. Both columns are identical and only differ by the coloring of the points. The left panel colors by the type of the secondary star, whereas the right panel colors the points by the inner eccentricity, e_1.

secondaries (orange points) become tidally circularized or mass-transferring at larger pericenter separations.

The right panel of Figure 2 colors the points by the inner eccentricity, e_1, showing that that about half of the systems halted at higher eccentricities, $e_1 > 0.9$. In this case, the tidal integration served to circularize and shrink them rapidly (on ~ 100 Myr timescales). For systems that were already circular (cyan points), the tidal prescription did not change their orbits. For highly eccentric systems, the pericenter actually increases slightly after tides because the system circularizes faster than it shrinks. For all points BH-LMXBs in the figure, high eccentricities ($e_1 > 0.9$) caused by EKL-induced oscillations from the distant tertiary led to angular momentum loss at close passages and eventual LMXB formation.

2.4. Example Formation of BH-LMXBs in Triples without Natal Kicks

In Figure 3, we show an example time evolution of a triple where the inner binary became an LMXB under the influence of the tertiary star's effects. In the first 10 Myr, the primary becomes a black hole. The mass loss from this event expands the orbits of the inner and outer binaries, which undergo secular eccentricity and inclination oscillations through the EKL mechanism. During this time, the inner orbit flips from prograde to retrograde and back multiple times, as shown in the second panel of Figure 3. The flipping, of course, is one of the hallmarks of the EKL mechanism, (Naoz et al. 2011). The eccentricity eventually gets pumped up to 0.9999, shrinking the pericenter distance to only ~ 6 R$_\odot$, within the secondary's Roche limit. At this
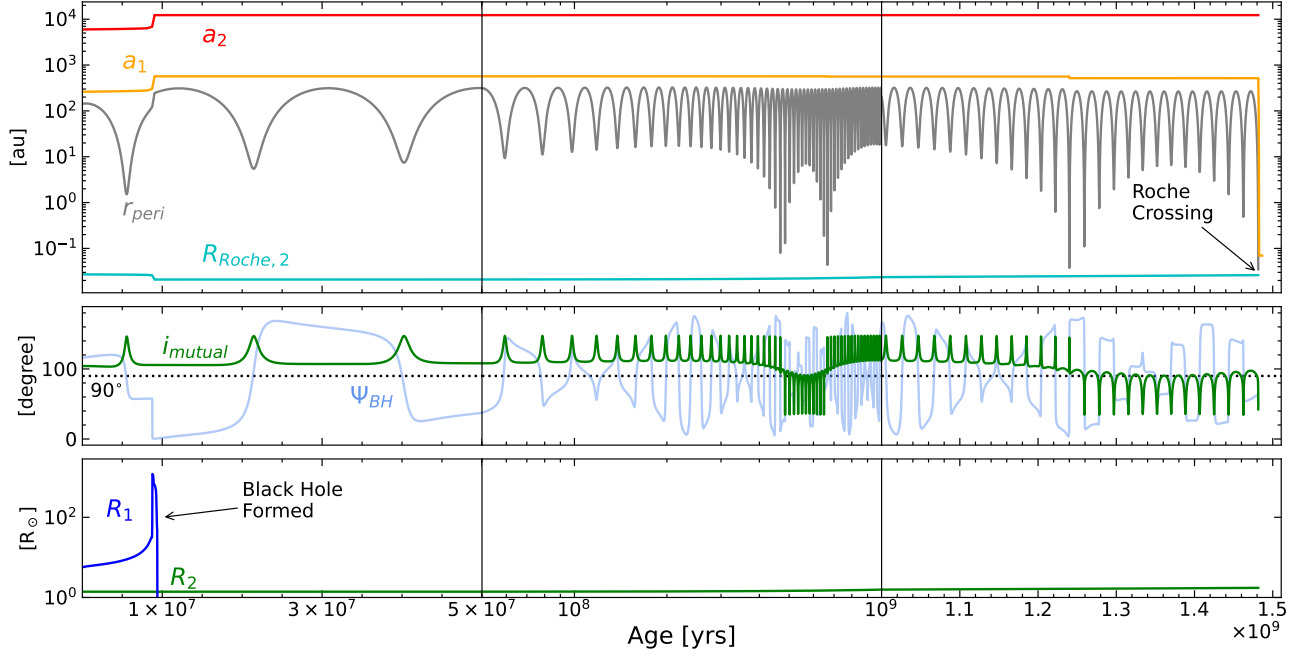
Figure 3. Time evolution of a triple system where the inner binary became an LMXB. **Top:** The evolution of the inner (a_1) and outer orbit (a_2) semi-major axes (orange and red), the pericenter distance ($r_{\rm peri}$, gray), and the Roche radius of the secondary in the inner binary ($R_{\rm Roche,2}$, cyan). **Middle:** The evolution of the mutual inclination ($i_{\rm mutual} = i_1 + i_2$) between the inner and outer orbits (green) and the spin-orbit angle of the black hole($\Psi_{\rm BH}$). Both angles are plotted in degrees. **Bottom:** The evolution of the radius of the primary (R_1, blue) and secondary (R_2, green) star in the inner binary. We label the moments where the primary star becomes a black hole ($\sim 10^7$ yrs) and when the inner binary crosses the Roche limit ($\sim 1.5 \times 10^9$ yrs). In the 500 Myr leading up to the RL crossing, the secondary star began to evolve off the main sequence with R_2 expanding 0.2 $R_\odot$. Throughout its evolution, the orientation of the inner binary flips multiple times between retrograde and prograde with respect to the outer orbit. At $t = 0$ the triples orbital and stellar parameters are $m_1 = 9.2\,M_\odot$, $m_2 = 1.45\,M_\odot$, $m_3 = 1.2\,M_\odot$, $a_1 = 261.3$ au, $a_2 = 5976.9$ au, $e_1 = 0.45$, $e_2 = 0.75$, $i_1 = 84.91°$, and $i_2 = 19.25°$. At the time of RL crossing, $e_1 = 0.9999$. Note that the time axes in the middle are log-scaled while the left and right panels are linearly scaled.

stage, the companion had only expanded by 0.2 $R_\odot$ from ZAMS.

At the point of RL crossing, the simulation terminates and we evolve the inner binary following Section 2.3. After only 1 Myr, the inner orbit tidally shrinks to $a_1 = 15\,R_\odot$ and circularizes to create an LMXB triple. Similar to V404 Cygni, this LMXB triple also has a circular inner binary and $a_1 \sim 0.1$ au. The final outer orbital elements are $a_2 = 12278$ au and $e_2 = 0.77$.

The particular system that we outline in this section formed from the "Eccentric" formation channel discussed in Naoz et al. (2016). Inner eccentricities above 0.9 are common for LMXB-forming systems within our sample, and 35% of all LMXBs reached eccentricities above 0.99. Notably, the triple formation channels that produce LMXBs through eccentricity pumping allow for initially wide inner orbits. Wide orbits that decay after BH formation generally avoid early interactions, which avoids the challenges associated with a CE event.

Since previous triple population synthesis studies used stellar prescriptions similar to those in SSE for single stellar evolution, we seek to understand how using SSE

would compare and affect the outcomes for this system. In Figure 8 in appendix A, we evolve the same initial conditions as shown in Figure 3, but include SSE single stellar evolution in the background (dash-dotted lines). With SSE, a 22 $M_\odot$ ZAMS star only becomes a $\sim 4\,M_\odot$ BH, and the triple does not produce an LMXB. The greater amount of mass loss in the inner binary expands the orbits, weakening EKL. Furthermore, the lower mass ratio in the binary suppresses octupole-level EKL effects, causing lower-amplitude oscillations (Naoz 2016, e.g.,). Correspondingly, SSE evolution causes the system to undergo small eccentricity-inclination oscillations after BH formation and remains detached for its entire evolution. On a population level, the larger stellar radii and smaller mass ratios derived from SSE would change the rates of BH-LMXB formation, though the direction of the trend is uncertain. To learn more about the differences between POSYDON and SSE in the context of triple dynamics, refer to Appendix A. All of the following results leverage POSYDON, which calls MESA grids, to evolve all stars in the hierarchical triples.

3. ORBITAL CONFIGURATION OF LMXB TRIPLES

3.1. *Without BH Natal Kicks*

In Figure 4, we plot the orbital configurations for triples with inner BH binaries at the final simulation timestep. The left column displays the simulations that do not include BH natal kicks, whereas the right column of the figure includes kicks. The color of each point corresponds to the stellar type of the BH companion in the inner binary. White dwarf, main-sequence, and red giant stars are colored blue, green, and orange, respectively. The square points represent BH-LMXB systems (see Section 2.2 for LMXB criteria). The small red points denote inner binaries that began RL crossing before the primary BH formed. Since our models do not self-consistently track CE evolution in triples, we simply show their orbital structure at the onset of RL crossing. Note that some of these systems may still become LMXBs, and in later sections, we investigate the outcomes of CE evolution among these inner binaries with POSYDON. In the right column, the x's show the orbital parameters of triples that became unbound because of the BH kick. Since they are no longer triples, we plot the orbital parameters just before the kick occurred. The star in the figure plots the observed inner and outer separation of V404 Cygni. We convert the outer separation of 3500 au into a semi-major axis following the results in Appendix B of El-Badry & Rix (2018), which accounts for different underlying eccentricities, inclinations, and observation angles. We conservatively choose the lower (upper) error to be a factor of $1/2 - 3$ times the separation. We consider any inner binary with these outer separations and closer than 0.2 au as 'V404 Cygni-like'. Note that we evolved systems that begin eccentric mass transfer using manual tidal evolution; refer to Section 2.3 and Figure 2 for the post-simulation tidal prescription. Among the systems that formed a BH in the inner binary without early mass transfer with the secondary, 14% become BH-LMXBs, and the rest remain detached.

We find that nearly all of the LMXBs with $a_1 < 0.2$ au have wide companions at separations of $2,000 - 10,000$ au, just like V404 Cygni. This contrasts with the wider systems ($a_1 > 0.5$ au) which have a broader distribution of tertiary companions between $10 - 10^4$ au. The difference in separations between these two populations effectively distinguishes their distinct evolutionary histories, which can be readily shown in Figure 2. The LMXBs with $a_1 \lesssim 0.1$ au in Figure 4 had wider orbits ($a_1 \sim 100 - 1000$ au) prior to mass transfer, yet experienced extreme eccentricities ($e_1 \gtrsim 0.999$) that made their periastron distances of order $a_1 \lesssim 1$ au (bottom row of Figure 2). At these distances, tides are dominant and rapidly shrink their orbit to become circular and end at similar separations to their periastron distance during the high eccentricity state (Figure 2). In most cases, the high eccentricities initiated RL crossing at periastron, often when the secondary star is a red giant (Figure 2, left column). The high eccentricities required for mass transfer in these systems highlight that their semi-major axes were above $100 - 1000$ au before the RL crossing. Therefore, their tertiaries are expected to be proportionally wider, at separations of $1000 - 10000$ au from the inner binary. This is precisely where the tertiary separations of LMXBs lie in Figure 4, and where the companion of V404 Cygni is today. Refer to Figure 3 for an example time evolution of such a triple.

For reasons explained above, nearly all BH-LMXBs in our sample with $a_1 \lesssim 0.1$ au harbor companions wider than 10^3 au, making V404 Cygni's orbital configuration consistent with forming via the triple channel. The separation of V404 Cygni's wide companion, 3500 au, hints that V404 Cygni likely came from an eccentric channel, where it was previously a wide, detached BH binary that reached extreme eccentricities while the secondary was a giant. At this stage, its orbit decayed significantly through angular momentum loss, either via tidal interactions or mass transfer. In the case of eccentric mass transfer, the systems may radiate in the X-ray, which can classify it as a partial (or micro-) tidal disruption event. Other dynamical channels show that such events can help probe BH populations in dense stellar environments (e.g., Perets et al. 2016; Fragione et al. 2019; Kremer et al. 2019; Fragione et al. 2020).

The slightly wider population of mass-transferring systems, with $a_1 \gtrsim 0.5$ au, circularized before mass transfer began. In these triples, the tertiary excites only moderately high eccentricities ($e > 0.9$) that do not cause mass transfer during the radial orbit, but tides still circularize and shrink the orbit during close pericenter passages. These tight, circular BH binaries begin to accrete after the secondary star expands, which is shown by the abundance of red-giant secondaries in this region (orange points, Figure 4). Stellar evolution of the BH companion plays a strong role in this pathway, which leads most of these systems to become these LMXBs after ~ 1 Gyr of triple evolution. In Table 3, we provide the number of LMXBs that formed through the different channels and different stellar types of their companions at the onset of mass transfer.

The separation of LMXBs is generally expected to decay over time as momentum is lost through accretion, outflows, gravitational waves, and magnetic braking (Paczyński 1967; Verbunt & Zwaan 1981; Tavani
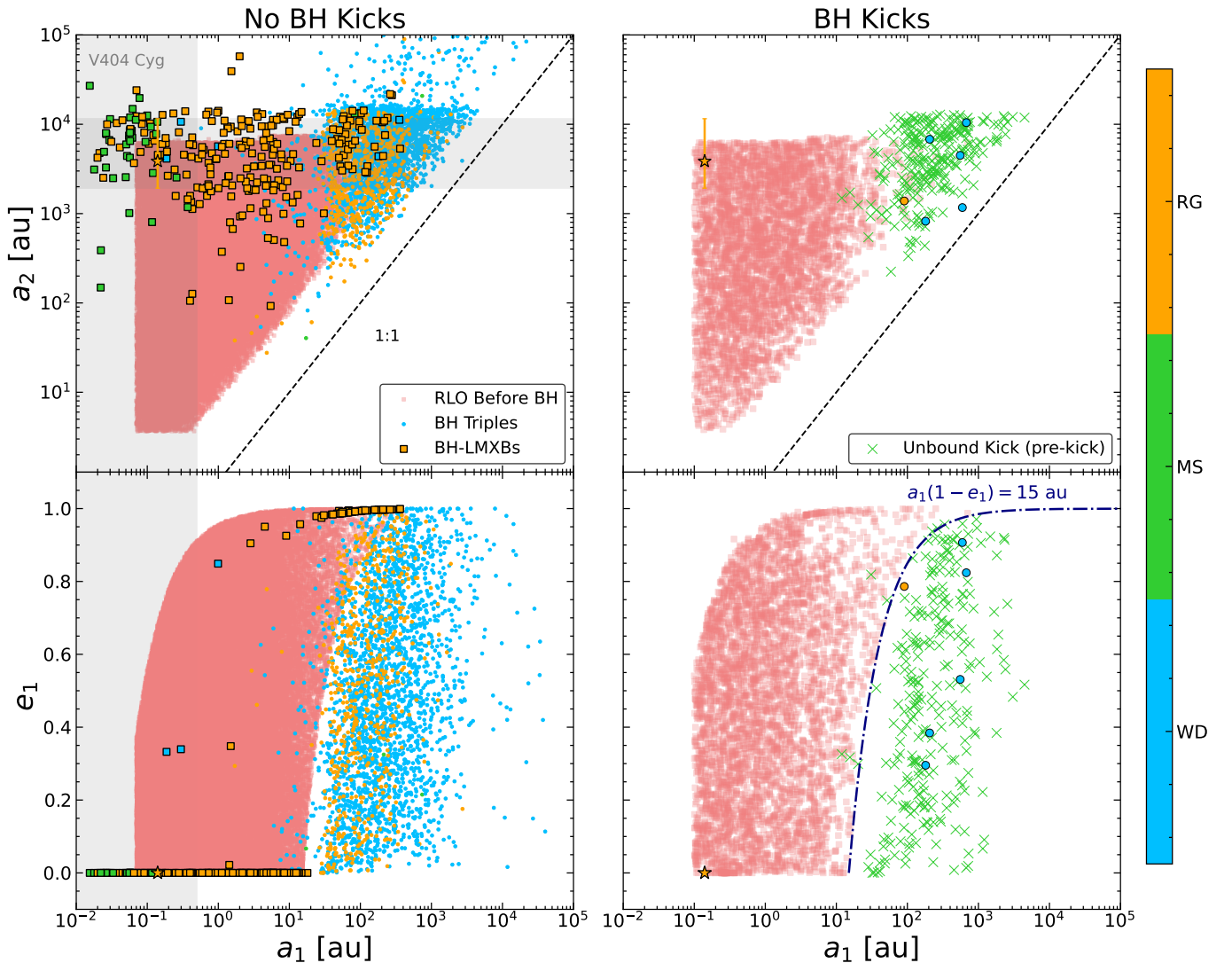
Figure 4. Outer-orbit's semi-major axis (a_2) and inner-orbit's eccentricity (e_1) as a function of inner-orbit's semi-major axis (a_1) at the last simulation timestep. The left column shows the results for simulations that do not include BH natal kicks, while the right column includes BH natal kicks. Red points underwent RL Crossing in the inner binary before the primary BH formed, and most are expected to merge as the result of a failed CE phase; we show their orbital configuration right before RL crossing. The rest of the points have one BH in the inner binary, and the color of these points represents the stellar type of the secondary star in the inner binary (its companion). The secondary stars are either main-sequence (MS, green), red giant (RG, orange), or white dwarf (WD, blue) stars. Circular points are detached BH inner binaries, while the squares are BH-LMXBs: BHs transferring mass with a companion star. The gray-shaded regions are the a_1 and a_2 observational constraints for V404 Cyg-like systems, which is also denoted by the star scatter point. We only show triples with tertiaries interior to 10^5 au since those wider than this cutoff would likely be unbound due to the Galactic tide. For the systems that became unbound (marked by x's), we plot the orbital configuration just before they became unbound. The kick velocities of the surviving systems range from $2 - 20$ km s^{-1}.

1991; Bahramian & Degenaar 2023, see latter for a re-
view). In our analysis, we do not consider the detailed
mass-transfer evolution of the LMXB after its initial
Roche crossing, so the separations discussed here will
be somewhat different than the current configurations
of observed LMXBs. The parameters analyzed here do,
however, give insight into the orbital structure of BH-
LMXBs before mass transfer and in their early stages.

3.2. *With BH Natal Kicks*

To test the impact of natal kicks in BH-LMXBs we
run 1642 Monte Carlo simulations that include BH for-
mation kicks (see Section 2.1.3 for the kick prescription).
We plot the final orbital configuration of these systems
in the right column of Figure 4. Among all simulations,
84% of the BH progenitors fill their Roche Lobe early on,
so those simulations terminate before a kick is induced
(small red points). The other 16% ($N = 270$) form
BHs, and only 6 of these triples (2%) remain bound
after the natal kick. 3 of the surviving systems had
$v_k \in 1 - 7$ km s^{-1} and the other 3 had $v_k \sim 20$ km s^{-1}.
The kicks for all systems ranged from $0 - 30$ km s^{-1} (see
Section 2.1.3), and the few that survived had precisely
aligned kick angles. Out of the systems that received a
kick and remained bound, none became a BH-LMXB,
and most of them evolved into detached BHWD inner
binaries with moderate eccentricities. From these sys-
tems alone, we find a 2% (6/270) probability that a
wide BH triple remains bound after even a relatively
small kick. The 6 triples that did survive the kicks had
similar inner and outer semi-major axes to the no-kick
BHs, though the eccentricities and inclinations change.
From the simulations without natal kicks, we find 14%
of triples that do not transfer mass before BH formation
become LMXBs. Overall, we find it highly unlikely that
any BH-LMXBs with a wide companion, which may be
a significant fraction of them (Naoz et al. 2016), formed
with a natal kick. If we take our initial conditions at
face value and assume a $5 - 10$ Gyr total evolution time,
we find that for every 10 detached BH binaries there ex-
ist ~ 1 V404 Cygni-like BH-LMXB (i.e., similar masses
and separations). At these rates, the triple channel may
be a dominant channel for forming BH-LMXBs (see Dis-
cussion in Section 3.4.2).

3.3. *The Evolutionary Timeline of V404 Cygni*

Previously we examined the different formation path-
ways of BH-LMXBs in hierarchical triples, and here, we
discuss the most likely scenario for V404 Cygni specif-
ically. We base this evolutionary history on the obser-
vation constraints that the donor is evolved, the age
is 4 ± 1 Gyr, and the current inner period is 6.4 days

(Shahbaz et al. 1994; Burdge et al. 2024). Initially, the
inner binary began wide ($a_1 \sim 10 - 100$ au) allowing
for the $20 - 30$ M$_\odot$ primary to evolve, which widened
the orbit even more from mass loss. After $\sim 10^7$ yrs,
the primary evolved into a BH without a natal kick,
forming a wide, detached BH+MS inner binary. Over
secular timescales, EKL-induced oscillations from the
tertiary ignited high eccentricities ($0.9 - 0.9999$) to the
inner binary. After $\sim 10^9$ years, the secondary began
to evolve off the MS, which allowed tides to shrink and
circularize the orbit during one of its radial expeditions
(e.g., Figure 3). Next, further post-MS evolution caused
the secondary to fill its Roche Lobe and begin trans-
ferring mass with the BH, creating a BH-LMXB. The
subsequent mass transfer and angular momentum loss
mechanisms likely further decayed the orbit, creating
the BH-LMXB structure that is observed today. The
age of V404 Cygni, the evolved state of the donor, and
the relatively wide period support this channel.

V404 Cygni could have also formed in through the
classical common envelope channel. In this scenario,
the role of the tertiary is less clear. If the inner binary
was initially tighter than ~ 15 au, then CE evolution
is likely to occur without much dependence of the ter-
tiary's dynamical influence. On the other hand, if the
initial separation of the inner binary was slightly larger
($20 - 100$ au), the tertiary could have excited the ec-
centricity of the inner binary through EKl oscillations,
leading the secondary to fill its Roche Lobe at perias-
trons. In the latter case, extra orbital energy will be
present the onset of CE, leading to a larger fraction of
binaries that survive the CE. However, our models show
that both CE channels allow for a wide range of a_2 val-
ues most of which are incocnsitent with the constrained
outer separation in V404 CYgni. For EKL-induced CE,
the median $\log_{10}(a_2 \ / \text{ au})$ is 2.27 with a standard de-
viation of 0.66, making this scenario unlikely for V404
Cygni, which has a $\log_{10}(a_2 \ / \text{ au})$ likely larger than 3.54
(3500 au Burdge et al. 2024). In the regular CE chan-
nel, without early EKL oscillations, there is no signifi-
cant preference for the outer semi-major axis other than
potential restrictions from stability. Also, if the rapid
non-adiabatic mass loss occurred during the envelope
ejection, which is likely (e.g., Ivanova et al. 2013), then
a small kick would be imparted on the triple, poten-
tially unbinding the wide tertiary. Given this scenario,
and that V404 Cygni's a_2 lies in the most probable range
for the triple channel without CE (Figure 4), we predict
that V404 Cygni most likely formed without a CE.

3.4. *Comparison to Binary Evolution Models*
3.4.1. *Efficiency of BH-LMXB Formation*

Table 2. Outcomes of Triple and Binary Population Synthesis

Outcome	Binary	Binary+Kicks	Triple	Triple+Kicks
	(%)	(%)	(%)	(%)
Merged	45.2	45.9	87.4	87.6
Disrupted	1.22	53.0	2.36	10.8
Detached BH	51.7	0.37	5.49	0.17
BH-LMXB	1.90	0.73	4.58	1.37

While V404 Cygni, among other BH-LMXBs, likely received no kick, others likely did. In this section, we aim to understand how kicks influence BH-LMXB formation in both triple and isolated binary channels.

Using POSYDON v1 (Fragos et al. 2023), we initialize a population of 20000 binaries, 10000 with BH natal kicks and 10000 without. The initial conditions are identical to the inner binary of our triple population. The primary mass is set to 21.7 $M_\odot$, which produces a ~ 9 $M_\odot$ for SN_STEP following Patton & Sukhbold (2020). The secondary mass is set to be uniform from $1.2 - 2$ $M_\odot$. The initial period is chosen from log-uniform with the period range of $0.1 - 10^4$ years, and we run all binaries for an upper limit of 10 Gyr with initially uniform eccentricities and solar metallicities. Similar to the triple simulations, the binary population with BH kicks follows the distribution from Hansen & Phinney (1997) normalized by the black hole mass (see Section 2.1.3). Binaries that are merged, disrupted, or unbound due to kicks halt before the 10 Gyr evolution time. When comparing the results of the binary population to the triples population, we specifically compare the inner binary of the triple to the isolated binary. This allows us to distinguish the role of the tertiary in forming BH-LMXBs.

In Table 2, we compare the statistical outcomes from the binary models to the triple models. The four populations include (1) Binaries without BH kicks, (2) Binaries with BH kicks, (3) Triples without BH kicks, and (4) Triples with BH kicks, where the triple populations are the same as analyzed in previous sections (Table 1). For all populations, if the periastron separation of the of BH progenitor with the secondary is less than ~ 10 au, the stars enter a CE phase. For the binary populations, with and without kicks, $\sim 45\%$ experience a CE. In the triple populations, $\sim 90\%$ experience a CE. The larger fraction of CE binaries in triples is attributed to the EKL mechanism. Namely, many triples experience early EKL oscillations that excite the inner binary's eccentricity to
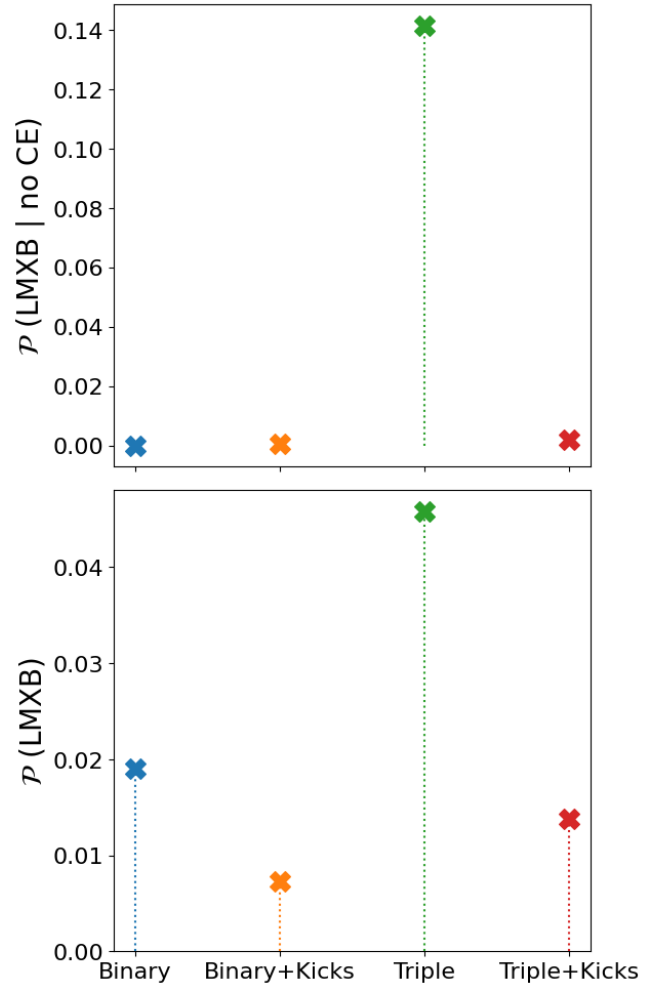
Figure 5. Percentage of BH-LMXBs formed in the different populations. The top row shows the percentage of BH-LMXBs out of all systems that avoided a CE, whereas the bottom row includes all systems in the model's population, including those that underwent a CE phase. Specific values for the bottom panel are listed in the last row of Table 2.

above 0.9 before the BH forms. The high eccentricities shrink the periastron distances of many wide inner binaries ($a_1 > 20$ au) to below the Roche Limit, placing them into a CE phase. In contrast to the binaries, these new CE binaries are wider, supplying more orbital energy for the secondary to eject the envelope of the BH progenitor. The large initial mass ratios ($m_1/m_2 \sim 20$) make the higher-order EKL effects particularly strong (e.g., Naoz et al. 2013a).

In $\sim 95\%$ of cases, the binary does not survive the CE. This fraction is consistent throughout both binary populations since the mass ratios and separations are similar. The remaining $\sim 5\%$ that survive the CE end up in tight ($\sim 10 - 100$ $R_\odot$) orbits, most of which become BH-LMXBs. In the kicks populations, many be-

come wide and eccentric from a natal kick, with another fraction unbinding completely. We note that our triples simulations halt when the inner binary begins Roche Crossing, meaning that we did not model the CE evolution for the $\sim 70 - 80\%$ of triples that experience a CE. However, since we ran a binary model with identical masses and separations, we identify the closest binary match and determine the mass transfer outcome for the inner binary based on the outcome from POSYDON. The outcomes of CE evolution include merging, remaining bound, or becoming unbound due to a natal kick. For the triples+kicks population, we use the CE outcome probabilities from the binaries+kicks populations, and for the triple population, we use the CE outcome probabilities from the binary populations. Assuming similar fractions between the models is not completely accurate because, as mentioned above, the triples more frequently enter a CE at separations wider than the isolated binaries. Therefore, we expect that more triples would survive a CE, given their additional orbital energies.

The second outcome shown in Table 2 are the binaries and triples that were made unbound by a natal kick (denoted as 'Disrupted'). For the populations with BH kicks, this occurred for $\sim 53\%$ of all the binaries and triples. The 1.22% (2.36%) of binaries (triples) that became unbound in the no-kicks population are due to forming neutron stars. Early mass transfer decreased the primary's mass, putting it below the threshold of forming a BH, making it an NS with a natal kick instead. In the binary+kicks population, the binaries that led to BH-LMXBs had kicks of $10 - 115$ km s^{-1} while the detached ones had smaller kicks ($0 - 50$ km s^{-1}). For the kick-surviving binaries, the pre-kick separations are bimodal about 0.5 au and 1.5 au with circular orbits. After the kick, the bound systems have roughly log-uniform separations between 1 and 100 au with moderate to high eccentricities. Overall, since most binaries completely unbind after a kick, the fraction of BH-LMXBs is lower on a population level compared to the no-kick binaries. However, among the minority of bound post-kick binaries, a significant fraction become BH-LMXBs due to their high post-kick eccentricities.

The second category of outcomes in Table 2 is the 'detached BH' which is the fraction of systems within a population that evolves as detached BH binaries, i.e., without ever exchanging mass. In the absence BH natal kicks, 51.7% of binaries remain detached, whereas in triples, only 5.49% remain detached. The lower detached fraction in triples because (1) more inner binaries had a CE, and (2) 14% of detached BH-binaries eventually transfer mass due to high eccentricities caused by the tertiary. When natal kicks are present, the detached

fractions are slightly lower than the respective models without kicks because a larger fraction of systems get disrupted, while the ones that survive generally have high eccentricities, leading to a greater mass transfer rate.

In the last row of Table 2, we show the fraction of systems that became BH-LMXBs in each population. Overall, the models without kicks produce a greater fraction of BH-LMXBs. Among all, the triples without kicks are the most efficient, with 4.58% of all systems becoming BH-LMXBs. This large fraction, relative to the binaries and kicks models, is due to the dynamical influence of the tertiary. Firstly, as previously discussed, a tertiary causes more inner binaries to undergo CE evolution at wider separations because it can excite eccentricities while the BH progenitor is evolving, causing close periapsis for binaries that would otherwise stay detached. While a small fraction of these systems survive, those that do are close and often become BH-LMXBs. The second reason for the efficiency of the triple channel is because $\sim 14\%$ of wide, detached BH+MS binaries, the tertiary causes high eccentricities that allow tides to shrink the inner orbit and eventually create a BH-LMXB. Therefore, the presence of a tertiary makes BH-LMXB formation $2 - 3$ times more efficient than isolated binaries (4.58% compared to 1.90%), when BH natal kicks are absent. With BH natal kicks, the triple channel is slightly more efficient because a larger fraction of inner binaries enter a CE, often at wider separations.

Figure 5 displays the efficiency of LMXB formation for the different channels. The bottom panel reflects the absolute fraction of BH-LMXBs in the population. The top panel shows the same fraction but only considers systems that avoid a CE. The outcome of a CE phase with a mass ratio of ~ 20 is uncertain, so we show the top panel in the case that all of such CEs result in a merger. Since most BH-LMXBs form after a CE, the only population that has a non-negligible probability of forming a BH-LMXB while avoiding a CE is the triple without kicks. In the next section, we leverage the rates in Table 2 and Figure 5 to compare our theoretical populations to the population of BH-LMXBs in the Galaxy.

3.4.2. *Number of BH-LMXBs in Galaxy*

We estimate the number of BH-LMXBs that currently exist in a Milky Way-like galaxy for each of our models, assuming our initial conditions. Considering a star formation rate (SFR) of 1 M$_\odot$ yr^{-1} and an LMXB lifetime of $\tau_{\mathrm{LMXB}} = 1$ Gyr, we apply the following equation,

which is an extension from Naoz et al. (2016):

$$N_{\text{BH-LMXB}} = \tau_{\text{LMXB}} \times \text{SFR} \times f_{m_1 > 20} \times f_q \times$$
$$f_{\text{binary/triple}} \times f_{\text{BH-LMXB}} \quad (8)$$

For all models, we set $f_{m_1>20} = 2/1000$ and $f_q = 1/20$, which are the fraction of stars above 20 $M_\odot$ assuming a Kroupa IMF (Kroupa 2001) and the fraction of systems with a mass ratio of 20:1 assuming a uniform mass ratio distribution (Sana et al. 2012), respectively. $f_{\text{binary/triple}}$ is the massive star binary fraction or the massive star triple fraction, depending on whether we are calculating for a binary or triple population. Since the BH progenitor is $\gtrsim 20$ $M_\odot$, we use $f_{\text{binary/triple}} = 0.35$ in the triple models and $f_{\text{binary/triple}} = 0.21$ in the binary models (Sana et al. 2012, 2014). All of the above fractions are independent of the outcomes from our models. The fraction of systems in the population that become BH-LMXBs, $f_{\text{BH-LMXB}}$, is taken from the outcomes of our population synthesis (last row of Table 2). Note that $f_{\text{BH-LMXB}}$ is inevitably a function of of our assumed initial masses and separations, making it prone to uncertainties.

Based on these statistics, we find that $N_{\text{BH-LMXB}} = 1603$ form in triples and $N_{\text{BH-LMXB}} = 400$ form in binaries, if BH natal kicks are not assumed. Combined, they predict a total of 2003 BH-LMXBs in the Galaxy if BHs are born without natal kicks. With kicks, the triple model predicts $N_{\text{BH-LMXB}} = 481$, and the binary model predicts $N_{\text{BH-LMXB}} = 153$, for a total of 634 BH-LMXBs in the Galaxy. If only a fraction of stellar BHs experience natal kicks, then one can adjust these numbers proportionally. For example, if half of the black holes have natal kicks, then $N_{\text{BH-LMXB}} = 1319$ in the Galaxy. Note that both with and without BH natal kicks, we predict that $\sim 80\%$ of BH-LMXBs in the Galaxy formed in triple star systems. If kicks are common, these tertiaries are unlikely to be bound today.

By modeling the spatial distributions and outburst recurrence timescales of Galactic BH-LMXBs, Corral-Santana et al. (2016) estimate that a total of 1280 ± 120 BH-LXMBs exist in the Milky Way. The above estimate assumes a mean outburst recurrence period of 100 yrs for the transients and relies on the fraction of these systems that have accurate distance measurements. Previously, White & van Paradijs (1996) and Romani (1998) respectively estimate ~ 500 and ~ 1700 BH-LMXBs in the Galaxy. All of these predictions also implicitly assume that undetected transients have comparable peak X-ray luminosities to those already observed, so the true number of BH-LMXBs still remains uncertain. Both the kicks and no kicks models are consistent with current estimates for the number of BH-LMXBs. Of course, our

population does not encompass the entire landscape of BH-LMXB progenitor masses, and studies with broader initial conditions can improve these estimates.

4. TIME OF LMXB FORMATION

As the age of a population increases, the mass of the donors in LMXBs is also expected to decrease (Fragos et al. 2013a,b; Lehmer et al. 2014). The age of V404 Cygni is constrained from isochrones to be 4 ± 1 Gyr (Burdge et al. 2024), and the present-day BH companion has lost at least 0.5 $M_\odot$, likely through accretion onto the BH (Burdge et al. 2024). Therefore, while the total age of the system is constrained, the precise time that mass transfer commenced, and the LMXB formed, is unclear. In this section, we investigate the time of initial mass transfer in our LMXBs (t_{LMXB}) and how it relates to various orbital properties.

In Figure 6, we display various binary properties against t_{LMXB}. The top panel shows the distribution of t_{LMXB}, the middle panel shows the pericenter distance (r_p) vs t_{LMXB}, and the bottom panel shows $1 - e_1$ vs t_{LMXB}. The color of the points corresponds to the radius of the secondary (donor) star in the inner binary. Bluer points mark less evolved, MS stars while the brighter purple points denote evolved giants. Note that the orbital parameters in this figure are at the time that the first mass transfer began between the black hole and its companion, which is often before tides have circularized the orbit.

Based on the left-skewed distribution, two populations of LMXBs arise: those with $t_{\text{LMXB}} > 10^9$ yrs ($N = 246$, 73%), and those formed before 10^9 yrs ($N = 92$, 27%). The panels below the distribution highlight that these different populations correlate to the stellar evolution of the donor star. Nearly all LMXBs with $t_{\text{LMXB}} > 10^9$ yrs have companions on the giant branch (Table 3). Among the LMXBs with donors on the giant branch, 49% tidally circularized before beginning mass transfer, and 35% began mass transfer while orbit was nearly radial ($e_1 > 0.9$). Those that circularized formed through a route similar to the "Giant" channel from Naoz et al. (2016), where moderately high eccentricities allowed tides and magnetic braking to shrink and circularize the inner orbit. Then, post-MS stellar expansion of the donor caused Roche Lobe filling and mass transfer, often at separations ~ 1 au. This channel uniquely requires stellar evolution of the donor star and occurs in 25% of LMXBs. This is a factor of 2 larger than predicted by (Naoz et al. 2016) and is likely attributed to our focus on masses similar to V404 Cygni. Secondaries with $m_2 \gtrsim 2$ $M_\odot$ would evolve in less than a Gyr, while most of those below $m_2 \sim 1.2$ $M_\odot$ would not

Table 3. LMXB Types at Initial Mass Transfer

Formation Channel	N	$t_{\rm LMXB}$	Donor Star Type		
		> 1 Gyr	MS	RG	WD
Radial ($e_1 > 0.9$)	131	91	40	87	4
Circular ($e_1 < 0.05$)	150	115	29	121	0
Other	57	40	14	40	3

become giants in a Hubble time. We also use POSYDON (Fragos et al. 2023), which has updated stellar evolution prescriptions compared to SSE (Hurley et al. 2000), which was used in Naoz et al. (2016).

Most of our systems became LMXBs after 1 Gyr, where most of the secondaries are at least slightly evolved stars (Figure 6). This matches closely with observations of V404 Cygni, which show that the secondary is evolved (Burdge et al. 2024). In these systems, the pericenter distance is generally larger since a more extended companion will have a larger Roche Lobe. Furthermore, half of the LMXBs with evolved companions tend to be circularized before mass transfer. In contrast, the LMXBs that formed before 1 Gyr primarily have main-sequence donors. They also possess smaller pericenter distances and more extreme eccentricities, which are required for mass transfer with smaller companions. V404 Cygni has the second most evolved donor among the ~ 25 BH-LMXBs known. Most BH-LMXBs have MS or slightly evolved MS stars with orbital periods less than 1 day. Selection effects may also favor short-period systems.

5. SPINS, INCLINATIONS, AND ECCENTRICITIES

Miller-Jones et al. (2019) observed that the orientation of V404 Cygni's jets are rapidly changing on the timescale to hours to minutes. It has long been theorized that a tilted disk, which is misaligned from the BH spin-axis, would undergo Lense-Thirring precession (Lense & Thirring 1918). Lense-Thirring precession is a general relativistic consequence of the rotation of a massive body, where the plane of the the orbit precesses about the spin vector of the black hole. For disks, this effect has been tested and confirmed numerically using magnetohydrodynamics simulations (Fragile & Anninos 2005; Fragile et al. 2007). X-ray outbursts of V404 Cygni are consistent with an optically thick, slim disk configuration (Motta et al. 2017), and the inferred mass accretion rate onto the BH implies an outer disk radius consistent for solid-body precession (Miller-Jones et al.
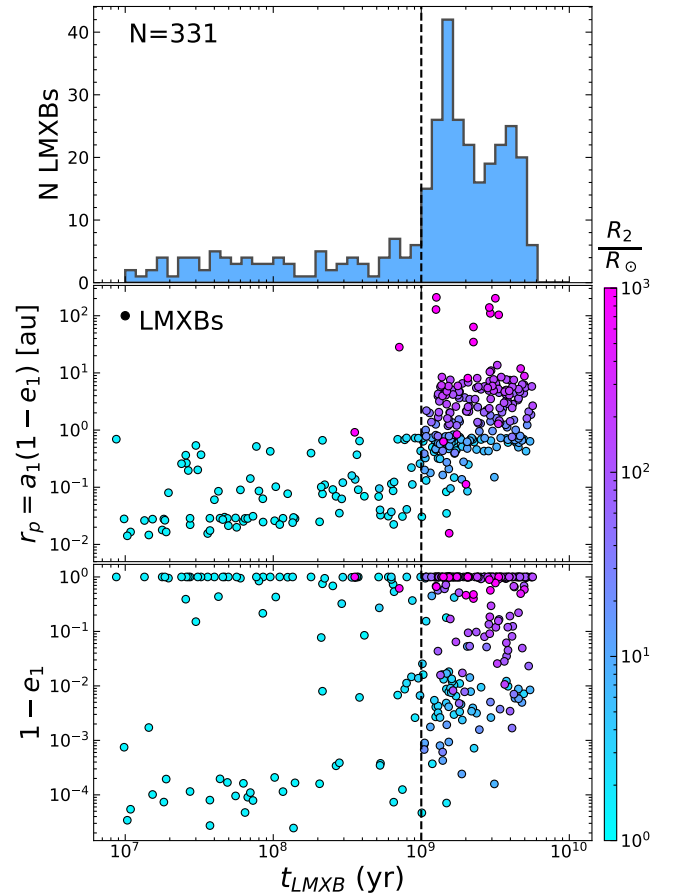
Figure 6. Characteristics of LMXBs at the onset of mass transfer. At the top, we show the distribution of $t_{\rm LMXB}$. In the middle panel, we plot the pericenter distance, $r_p = a_1(1 - e_1)$, at the time of LMXB formation ($t_{\rm LMXB}$) as a function of $t_{\rm LMXB}$. In the bottom, we plot $t_{\rm LMXB}$ vs. $1 - e_1$ at $t_{\rm LMXB}$. The magenta points are red giant (or evolved) BH companions, while the bluer points have MS companions in the LMXB. The black dashed line marks 1 Gyr. The LMXB population can be divided into the population that formed before/after 1 Gyr.

2019). Therefore, the precession of the disk in V404 Cygni is consistent with Lense-Thirring precession. We note that these results are somewhat model-dependent and assume intrinsic jets when interpreting the X-ray data. The significance of this assumption, and therefore the results, remains unclear. This supposed misalignment between the BH spin and the binary orbital place of the LMXB was previously attributed to a supernova kick in V404 Cygni (Miller-Jones et al. 2009, 2019) and other BH-X-ray binaries (e.g., Atri et al. 2019). However, from the presence of a distant companion and the kick analysis performed here and in Burdge et al. (2024), V404 Cygni almost certainly formed without a BH natal kick.

EKL oscillations in hierarchical triples naturally lead to spin-orbit misalignments before the onset of mass transfer(Naoz & Fabrycky 2014; Liu & Lai 2017; Su et al. 2021). Over secular timescales, the inner binary oscillates through a wide range of inclinations, as we illustrate in the second panel of Figure 3. When the mass transfer between the BH and its companion begins, the newly-formed LMXB will generally maintain a similar inclination and thereby be misaligned with the BH spin. Here, we examine the angle between the BH spin and the binary orbit, the spin-orbit angle (Ψ_{BH}), at the initial formation of the LMXB.

In Figure 7, we plot e_2, the eccentricity of the outer orbit, against Ψ_{BH}, the spin-orbit angle of the black hole (in degrees). The points are colored by the mutual inclination of the triple, and the distributions for Ψ_{BH} and e_2 are plotted adjacently. In nearly all cases, triple dynamics will cause a misaligned BH spin-orbit angle in BH-LMXBs. The distribution of Ψ_{BH} is roughly isotropic, with the most likely misalignment angles being between $45° - 135°$. In the classic formation channel, where LMXBs form in isolated binaries, a primordial BH progenitor undergoes a CE phase with its companion (e.g., Tauris & van den Heuvel 2006b). Up to this event, the BH progenitor expanded significantly, where tidal interactions would have slowed down and synchronized the primary's spin axis with the orbit. Since it is not generally expected that the CE evolution will break the corotation (Ivanova et al. 2002; Taam & Ricker 2010; Ivanova et al. 2013). Under this channel, assuming no BH kicks, the BH spin will therefore be aligned with the binary orbit, unlike what is observed in V404 Cygni.

The three-body systems that produce BH-LMXBs slightly disfavor circular outer orbits, $e_2 \lesssim 0.2$, because higher order EKL effects are weaker in this regime (e.g., Naoz 2016). In fact, we find that LMXB-producing triples mainly had initial outer eccentricities of $e_2 \sim 0.4$ or $e_2 \gtrsim 0.7$ (Figure 10). From the same figure, we find that these systems also had initial mutual inclinations near $90°$, meaning the inner and outer orbit were perpendicular at $t = 0$. Initially, perpendicular orbits and moderate outer eccentricities both strengthen the amplitude of EKL eccentricity/inclination oscillations in the inner binary of the triple Naoz et al. (2013a); Naoz (2016). Since the most common LMXB evolutionary pathways in triples include high eccentricities ($\gtrsim 0.95$), such inclinations and eccentricities for the outer orbit are favorable. In its final state, most LMXBs have only moderate mutual inclinations, $|\cos i_{mutual}| \sim 0.7$, which maps to values of i_{mutual} near $45°$ and $135°$.

From the results of our MC simulations that test a wide range of orbital arrangements, we predict that nearly all BH-LMXBs formed through the triple channel will have (1) misaligned BH spin-orbit angles with (2) moderate inclinations and outer eccentricities, irrespective of whether a kick was present or not. We also show that the initial mutual inclination of the triples that form BH-LMXBs is almost always near $90 \pm 10°$. Our prediction for Ψ_{BH} is at the onset of mass transfer, and we do not consider mechanisms that could change Ψ_{BH} during the LMXB evolution. We note that misaligned spins from triples equally include retrograde and prograde spins relative to the binary orbit. Interestingly, Morningstar et al. (2014) claim that GS 1124-683, a BH-LMXB, has a retrograde accretion disk. In contrast to the BH, the donor star is expected to have an exceedingly small spin-orbit angle that has been decayed through mostly tidal evolution (e.g., Naoz & Fabrycky 2014; Toonen et al. 2016), which we also find in our simulations. V404 Cygni has already accreted at least $0.5 \ M_\odot$ of material from the companion star (Burdge et al. 2024), so any mechanisms that would align initially misaligned orbits would likely have taken place on timescales shorter than its total time of accretion (e.g., Maccarone 2002; Martin et al. 2008; Steiner et al. 2012; King & Nixon 2016). Beyond V404 Cygni, future observations of a misaligned disk or jet, in the absence of natal kicks, could support the triple formation channel, and perhaps the presence of a hidden companion.

6. DISCUSSION

As shown here, EKL oscillations enable wide BH inner binaries ($20 - 1000$ au) to tighten and interact, either by avoiding a CE phase altogether or by increasing the likelihood of successful envelope ejection by initiating the CE at wider separations. Another possibility is that the inner binary in V404 Cygni evolved through a CE phase but with minimal dynamical influence from the tertiary. While this scenario is possible, the observed V404 Cygni's tertiary separation of 3500 au is among the most probable values predicted by the classical triple channel (Figure 4). This supports that the inner binary of V404 Cygni was initially wide and brought together through EKL migration, either before the BH formed – implying a CE phase – or after, in which case no CE occurred.

Further, we show that BH-LMXBs that currently reside in triples likely did not receive a BH natal kick or, at most, received a negligible one. Our triple models assume general initial separations but only consider masses similar to V404 Cygni, though these masses are typical for many observed BH-LMXBs (Corral-Santana et al. 2016). Although dynamically difficult, the presence of a natal kick in BH-LMXB triples is not impossi-
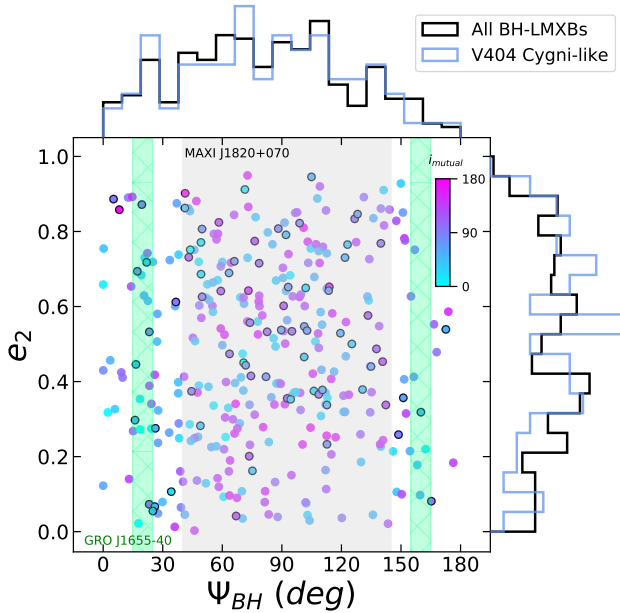
Figure 7. Predictions for the eccentricity of the outer orbit (e_2) and the spin-orbit angle of the inner black hole (Ψ_{BH}). We color the points by the mutual inclination of the triple, which is mostly likely be near $45°$ or $135°$ (e.g., Figure 10). If an LMXB is outlined in the plot, then it is classified as being V404 Cygni-like, meaning $a_1 < 0.5$ au and $a_2 > 2000$ au. Interestingly, the Ψ_{BH} distribution is roughly isotropic, implying that most BH-LMXBs formed in hierarchical triples are expected to be misaligned. V404 Cygni, for example, has a likely spin-orbit misalignment, as suggested by the changing orientation of its jets (Miller-Jones et al. 2019). The gray and green regions respectively display constraints for the spin-orbit angle of the BH-LMXBs MAXI J1820+070 (Poutanen et al. 2022) and GRO J1655-40 (Martin et al. 2008).

ble. Some BH-LMXBs have been constrained to experience kicks of at least tens of km s^{-1}, often by combining peculiar velocity measurements with galactic orbits and binary evolution models (e.g., Fragos et al. 2009; Kimball et al. 2023; Mata Sanchez et al. 2024). Currently, the distribution of BH natal kicks is not well understood. Some BH-LMXBs seem to have experienced substantial kicks, ($\gtrsim 80$ km s^{-1}, e.g., Fragos et al. 2009; Repetto et al. 2012; Repetto & Nelemans 2015; Repetto et al. 2017; Mandel 2016; Kimball et al. 2023; Mata Sanchez et al. 2024) as often inferred from their high peculiar velocities. Others, including V404 Cygni, likely did not receive any significant natal kicks (e.g., Mirabel & Rodrigues 2003; Wong et al. 2012; Reid et al. 2014; Mirabel 2017; Shenar et al. 2022; Vigna-Gómez et al. 2024; Burdge et al. 2024). This discrepancy points to a potential bimodality in the BH kick distribution, where some BHs form with extremely weak to null kicks, while others do

not (see Nagarajan et al. 2024, in prep.). Here, we provide additional support that some stellar BHs that form without a natal kick. This fraction may be large if a significant number of BH-LMXBs are in hierarchical triples today. The orbits of observed detached BH+luminous companions binaries also support the absence of strong BH natal kicks (El-Badry et al. 2023a,b; Wang et al. 2024).

Assuming no BH kicks, we outline the possible separations and orientations of tertiaries to BH-LMXBs (Figure 4, 7, and 9). These updated constraints may guide future observations of BH-LMXBs in triples. Nonetheless, detecting BH-LMXB tertiaries remains challenging with current instrumentation. There are ~ 25 dynamically confirmed BH-LMXBs (e.g., Tetarenko et al. 2016; Corral-Santana et al. 2016), most of which are farther and less optically bright than V404 Cygni. The tertiary in V404 Cygni would not have been detected as a *Gaia* proper motion companion if it had been only ~ 1 kpc farther. As Burdge et al. (2024) mention, if the tertiary were only 10% more massive, it would have already been a WD, rendering it too faint for detection. If it were 0.5 M$_\odot$ less massive, then its absolute G-band magnitude would be below the *Gaia* detection limit, and if it were only 0.2 M$_\odot$ less massive, it would not have a precise proper motion measured (Burdge et al. 2024). Considering these limitations, we believe that it is highly possible that most BH-LMXBs formed in hierarchical triples, a conclusion that is also supported by our analysis.

Since LMXBs are associated with older stellar populations (e.g., Zhang et al. 2012; Lehmer et al. 2014) and the tertiaries are generally wide (Figure 4), small perturbations on the system may unbind the outer binary. These effects include galactic tides (e.g., Kaib & Raymond 2014; Grishin & Perets 2022), stellar flybys (e.g., Michaely & Perets 2020)[2], or WD birth kicks, (e.g., El-Badry & Rix 2018; Shariat et al. 2023). Also, if BH-LMXBs in triples experience a CE, rapid non-adiabatic mass loss is likely to occur (e.g., Ivanova et al. 2013), which could unbind wide (~ 1000 au) tertiaries.

In this study, we assume that highly eccentric systems that cross their Roche Limit at periastron will rapidly circularize and become BH-LMXBs (e.g., Figure 2). Currently, the outcomes of eccentric mass transfer are not entirely understood, and some of these binaries could instead manifest as micro-TDEs rather than BH-LMXBs (e.g. Perets et al. 2016). Still, a larger fraction

---

[2] Although in some cases these fly-by's can even lead to the formation of BH-LMXBs (Michaely & Perets 2016).

of BH-LMXBs in our triple models are already circularized before they begin mass transfer (Table 3). Also, though we upgraded our triple dynamics simulations to include new single stellar evolution models, we still do not self-consistently track binary mass transfer within the triple. To estimate the outcomes of an inner binary CE phase, we use POSYDON. Compared to older binary evolution codes, POSYDON's detailed angular momentum modeling has shown to be a somewhat improved model, especially for Be X-ray binaries (e.g., Rocha et al. 2024).

Our predicted rates for BH-LMXBs in the Galaxy are highly dependent on the results of CE evolution from POSYDON, which predict that $\sim 92\%$ of the CE binaries will merge. At the separations and mass ratios considered here, it may be the case that essentially all CEs lead to a merger when the mass ratio is 20. In this scenario, the triple channel without kicks would continue to produce BH-LMXBs efficiently, while the binary and kick models would not (top panel of Figure 5). Future investigations are required to constrain the outcomes of CE evolution and shed light on the formation pathways of LMXBs.

7. CONCLUSIONS

The recent detection of a wide companion orbiting V404 Cygni has allowed for a unique opportunity to test the formation and evolution of BH-LMXBs. Specifically, the presence of the tertiary requires the BH to have formed with a very weak kick and may support three-body formation channels for LMXBs. Here, we test both of these hypotheses by evolving a large grid of dynamical three-body systems and comparing them to a binary population from POSYDON. We revise our triple dynamics code by incorporating single stellar evolution MESA tracks, using POSYDON. Compared to older codes, these models use improved prescriptions that include full stellar structure modeling and are consistent with MESA stellar evolution, (Fragos et al. 2023). This treatment yields more realistic radii for evolved massive stars compared to SSE, which alters the evolution and outcomes of triple star systems (see Figure 8). Though we focus on V404 Cygni as a case study, the stellar and orbital parameters considered here are quite general and may be applied to a broader BH-LMXB population. Our main conclusions are summarized as follows:

1. *Outer separation distribution of BH-LMXBs in triples:* We show that when BH-LMXBs form through the classical triple channel, without a CE phase, the tertiary will have typical separations between $10^3 - 10^4$ au (Figure 10). If a CE occurred, then the tertiary's separation is less constrained, but generally is $\sim 100 - 1000$ au (see Section 3).

2. *BH-LMXBs in triples likely form without black hole natal kicks:* Our analysis shows that BH-LMXBs in hierarchical triples likely experienced no BH natal kicks, or at most, weak ones (with $v_{k,max} \leq 5$ km s^{-1}; see Figure 4). For V404 Cygni, we derive a $< 0.2\%$ likelihood that the BH formed with even a small natal kick ($\lesssim 30$ km s^{-1}).

3. *The triple channel produces BH-LMXBs more efficiently than isolated binaries:* By comparing our population of triples to a binary population from POSYDON, we find that triple evolution is the dominant formation pathway for BH-LMXBs. In triples, the fraction of LMXBs formed increases by a factor 2.5 (2) without (with) natal kicks, assuming an equal number of binaries and triples (Table 2). However, assuming a triple fraction of $\sim 35\%$ (e.g., Sana et al. 2012, 2014), a galactic stellar population may yield that 80% of BH-LMXBs form in triples (see Figure 5 and Section 3.4.2.) While this estimate relies on our assumed initial masses and separations, it applies irrespective of whether BH kicks occur in the system. The boosted rates of LMXB production in triples are attributed to two factors. First, early EKL oscillations spark high eccentricities, leading twice as many binaries to cross their Roche Limit and enter a common envelope with the BH progenitor, when compared to isolated binaries. In triples, these Roche crossings typically occur at wider separations with larger orbital energies. Second, when the tertiary remains bound, it can induce secular EKL torques to the inner BH binary, which brings together 14% of wide, detached BH binaries (e.g., Figure 3). Note that even with strong kicks, this first mechanism dominates, but the tertiary would have since been unbound from the system. In the pessimistic case, where nearly all CE phases with the BH progenitor lead to a merger, then the no-kicks triple scenario is the only significant contributor to LMXB formation among the channels considered here (top panel of Figure 5). Even in this regime, the wide tertiary may become unbound following galactic tides and fly-by interactions with field stars (e.g., Kaib & Raymond 2014; Grishin & Perets 2022; Michaely & Perets 2020).

4. *The orbit and orientation of BH-LMXB tertiares:* We constrain the possible tertiary orbits at birth and at BH-LMXB formation (Figure 10). The triple formation channel predicts that the current-day BH-LMXBs likely formed after 1 Gyr (Figure 6, and their tertiaries most probably have wide

separations (1000 – 10, 000 au) with moderate mutual inclinations (40° or 140°) and eccentricities (0.3 – 0.8). Additionally, the spin of the BH in BH-LMXBs, if formed in a triple, will generally be misaligned with the binary orbit at the onset of mass transfer (Figure 7). If the spin does not align quickly, the misalignment may manifest observationally as a retrograde accretion disk (e.g., Morningstar et al. 2014) or as rapidly changing jet orientations, which was claimed in V404 Cygni (Miller-Jones et al. 2019). If we consider inner binaries that underwent a common envelope, then the outer orbit is less constrained.

8. ACKNOWLEDGEMENTS

APPENDIX

A. POSYDON VS SSE SINGLE STELLAR EVOLUTION

In Section 2.1.2, we discuss our use of POSYDON for modeling the single stellar evolution for all three stars in the triples. In summary, POSYDON is a binary evolution code that leverages extensive grids of single- and binary-star models based on MESA. The code also implements state-of-the-art interpolation and postprocessing methods, which self-consistently evolve single and binary systems (Fragos et al. 2023). The major advance of POSYDON for single stellar evolution, as opposed to older codes such as SSE or COSMIC, is their accurate treatment of massive stellar evolution: i.e., stars that become black holes or neutron stars. Some key changes include updated recipes for stellar winds and core-collapse supernovae, both of which have modular aspects in the code. For the analysis in this paper, we have one massive star in the triple at ZAMS – the primary BH progenitor – so we explore the morphological differences between using POSYDON vs SSE. In Figure 8, we plot the time evolution for the same initial conditions as Figure 3, but model single stellar evolution using SSE (dash-dotted lines).

With SSE, the three-body evolution completely changed to create a widely different outcome than the original evolution. The main difference comes from the mass loss effects since the ~ 22 $M_\odot$ primary only produces a 4 $M_\odot$ BH. This resulted in a weakened impact of the tertiary on the inner binary, which causes only modest EKL oscillations over Gyrs. Furthermore, the result of this evolution was a widely detached (1000 au) BH binary, unlike the mass transferring BH binary produced with POSYDON+triple evolution. To learn more about the detailed, self-consistent stellar models in POSYDON, refer to (Fragos et al. 2023).

B. TIDAL EVOLUTION OF THE INNER BINARY BEFORE LMXB FORMATION

As discussed in Section 2.3, some of the simulations get computationally expensive when an evolved secondary star is on a highly eccentric orbit in the inner binary. Over half the time, the internal tidal prescription in the code evolves and circularizes these binaries rapidly. However, in a fraction of systems, the simulations slow down significantly at this stage. On timescales shorter than stellar evolution, tides will often dissipate orbital energy, which will shrink the inner orbit and make it circular. In highly eccentric orbits, as are present here, tides are especially efficient during the close pericenter passages. We, therefore, manually evolve the inner binary using the tidal equations above. Since no mass loss is involved, the tertiary separations remain the same throughout this process.

In Figure 2, we show the impact of the manual tidal evolution in altering the inner binary configuration for systems that became mass transfer LMXBs. The pericenter distance of the inner orbit ($r_p = a_1(1 - e_1)$) is plotted on the horizontal axis while the semi-major axis of the outer orbit (a_2) is plotted along the vertical axis. The top panel shows the initial-final periastron distribution. The second panel shows the periastron of the triples at the stop time of the triple code, where the color denotes the inner eccentricity (e_1) and the squares denote LMXB-forming triples. The bottom panel is the same as the second, but after applying manual tidal evolution. In the bottom panel, we also plot arrows denoting the direction of evolution for each of the LMXBs. In general, since the tidal evolution circularizes the
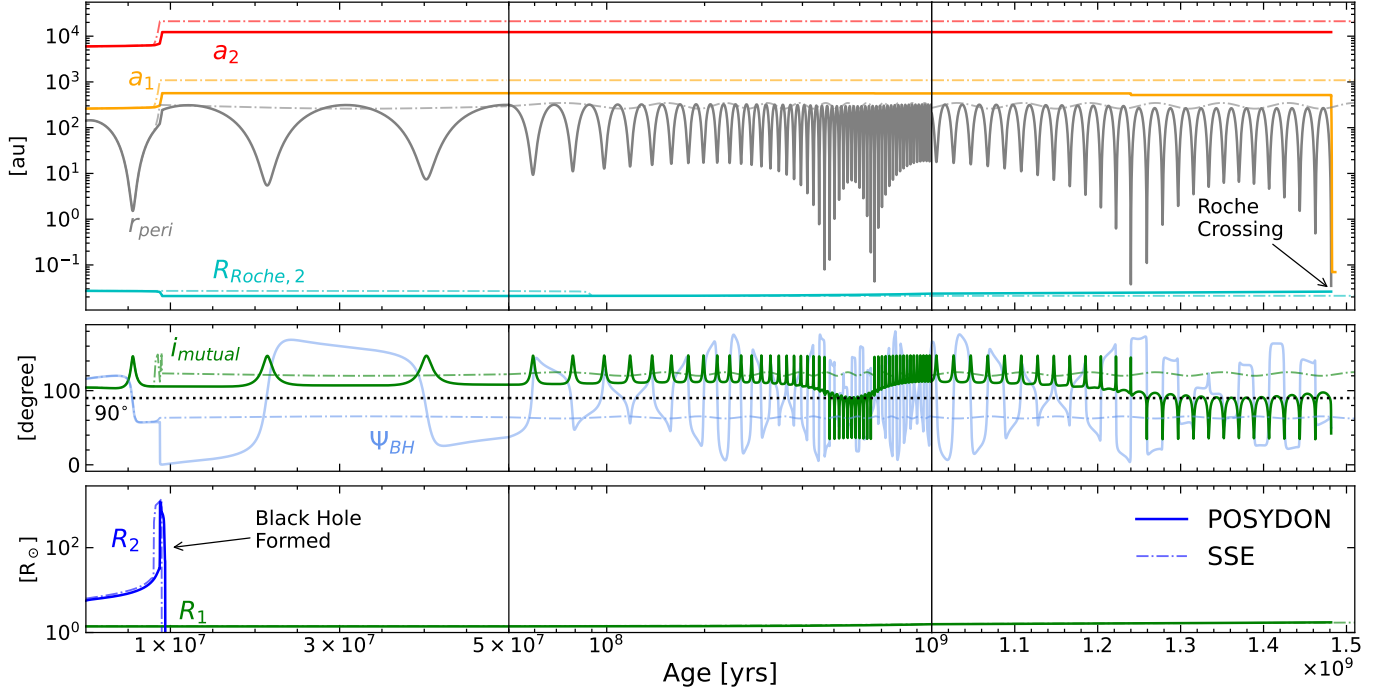
Figure 8. POSYDON vs SSE single stellar evolution as implemented in the complete triples dynamics code. This figure is the same system as Figure 3, but the dashed points show the same system evolved using SSE.

orbits, the periastron distance for already-circular orbits does not change. For the bright pink systems, which have high eccentricities $(0.9 - 0.9999)$, tides decrease their semi-major axis (a_1) while also taking e_1 to 0. The balance between the decreasing (a_1) and the increasing $1 - e_1$ generally results in an inner binary orbit that is slightly larger than the initial periastron distance at high eccentricities (bottom panel). One example is shown with the black arrow in the bottom panel, where a triple with $1 - e_1 = 10^{-6}$ and $a_1 = 13621.72$ au tidally decayed over a few periastron passages into $1 - e_1 = 1$ $a_1 = 0.16$ au. As shown in this example, highly eccentric binaries that were stopped in the code circularize quickly $(e_1 \lesssim 0.01)$, which makes the pericenter effectively equivalent to a_1. Although the tidal evolution generally occurs on $1 - 100$ Myr timescales, which is often shorter than stellar evolution timescales, there is a possibility that the secondary star will expand significantly during the tidal evolution. In this case, an eccentric mass transfer would occur, which can change the orbital structure (e.g., Sepinsky et al. 2007; Dosopoulou & Kalogera 2016; Hamers & Thompson 2019), especially within the context of triple dynamics (e.g., Toonen et al. 2016, 2018; Hamers & Thompson 2019). We do not follow the detailed mass transfer physics, though mass transfer could likely help remove angular momentum more rapidly (Hamers & Thompson 2019). This would not only create the an LMXB, or Symbiotic binary, at an earlier time but can further help shrink and circularize the orbit. Note also that an expanding stellar radius makes tides exponentially more efficient, which would further compound angular momentum loss (Equation 6, 7).

C. INITIAL-FINAL RELATIONS FOR BH-LMXBS WITH WIDE COMPANIONS

Among our entire population synthesis of BH triples, approximately 10% of the detached BH inner binaries began transferring mass while the secondary was an MS or RG star, rendering the system a BH-LMXBs. Among these mass transferring systems, 13% $(N = 42/375)$ have $a_1 < 0.5$ and $a_2 > 1000$, giving them similar orbital configurations to the V404 Cygni hierarchical triple. One of our goals from the population of triples is to examine the relationship between the initial and final orbital parameters, focusing on systems that form BH-LMXBs and V404 Cygni-like triples. In Figure 9, we display a corner plot that includes the initial (horizontal) and final (vertical) orbital parameters of the triples, which include a_1, a_2, e_1, e_2, and i_{mutual}. We outline the BH-LMXBs in black and color each point by their final eccentricity, shown in the third row. Since these are the orbital parameters at the onset of initial mass transfer, we again see two distinct populations based on their final a_1 values. The systems with $\log_{10}(a_{1,f} / au) >\gtrsim 1$ are mostly all highly eccentric, while those with $\log_{10}(a_{1,f} / au) \lesssim 1$ are nearly all circular. The latter population likely

also experienced moderately high eccentricities ($e_1 > 0.9$), but became tidally circularized before mass transfer began. This population is most often associated with evolved secondaries in the inner binary since the secondary's expansion most often initiated Roche Lobe crossing (see Figure 4).

Another notable feature of Figure 9 is the mutual inclination distribution for the BH-LMXBs compared to the general population of BH triples. The initial mutual inclination for BH-LMXB forming triples has a strong preference for $i_{mutual} \approx 90°$ (also see Figure 10, last column). At 90°, EKL-induced perturbations to the inner binary are enhanced, both to the quadrupole and octupole level (e.g., Naoz et al. 2013a). The bimodality in the final mutual inclinations, $i_{mutual,f}$, is observed in both populations (Figure 10, last column), but is more pronounced in the BH-LMXB population. We show the histograms from the aforementioned orbital parameters in the initial-final histograms shown in Figure 10.

Here, the gray distribution shows all BH Triples, the blue shows BH-LMXBs, and the green dashed histogram shows BH-LMXBs with triple orbital configurations similar to V404 Cygni ($a_1 < 0.5$ au and $a_1 > 2000$ au). Similar to the previous Figure, all of the data shown here is at the onset of mass transfer in from the simulations. This means that all BH+MS and BH+RG mass transferring systems are categorized as BH-LMXBs because their periastron decreases after tidal evolution. The criteria for being 'V404 Cygni-like' is for the post-tides orbit, so some V404 Cygni-like triples have large a_1 values before tides (e.g., column 1 in Figure 10). These systems have correspondingly high eccentricities caused by secular dynamics from the tertiary, making their periastron distances near the Roche limit of the binary. Within in each column, the histograms have the same bins.

From this plot, we can make several predictions about the initial orbital structure of triples that produce BH-LMXBs and the subset of which shape into V404 Cygni-like systems. Firstly, in a_1 distribution, all BH-LMXBs have preferred initial separations around $a_1 \sim 60$ au ($\log_{10}(a_1 \,/\, au) \sim 1.8$), slightly smaller than the total population of detached BH Triples. The final a_1 distribution is bimodal for the BH-LMXBs, while it is roughly Gaussian for the general population. The bimodality reflects the two formation channels, where the closest inner binaries often circularized prior to mass transfer and only began transferring mass when the secondary evolved into Roche Lobe filling. In contrast, the widest systems began mass transfer on a high eccentricity excursion, as noted by the final e_1 distribution (column 3). In fact, most V404-like systems, and most BH-LMXBs in general, formed from this channel, where extreme eccentricities led to close pericenter passages, which either initiated mass transfer or rapid tidal locking.

For the outer orbits semi-major axis (a_2), the BH-LMXB forming triples have closer separations to the inner binary, which cause stronger eccentricity excitations. The V404 Cygni-like BH-LMXBs initially have a sharp peak around $a_2 \sim 3000$ au, which is also the most common outer separation for all BH triple. The higher concentration of outer separations in this region also reflects that the surviving inner binaries were wide, requiring proportionately wide outer binaries for long-term stability. The initial inner eccentricities for all BH-LMXBs have a slight preference for larger values, which would allow for even small oscillations to ignite stellar interactions. For e_2, BH-LMXBs are most often formed with outer eccentricities around 0.3 and 0.8, especially for triple that become V404 Cygni-like. Since the angular momentum of the outer orbit is larger than the inner orbit's, these eccentricities are relatively conserved throughout the secular evolution, so the final e_2 values are also moderate. From the green curves in this column, we predict that V404 Cygni's outer tertiary began with $e_2 \sim 0.3$ or $e_2 \sim 0.8$ and today has a most-probable eccentricity in the range $e_2 = 0.3 – 0.9$. Relative to our entire population of LMXBs, V404 Cygni has a very common orbital architecture in nearly all regards. Many BH-LMXBs may harbor distant companions that are not yet resolved or have since been unbound. Although the initial conditions vary slightly from those in Naoz et al. (2016), the predictions made here are largely consistent with their study. The narrower range of masses studied applies more directly to V404 Cygni, and therefore, the time of LMXB formation changes slightly. Also, Naoz et al. (2016) use SSE, which can give qualitatively different outcomes that POSYDON (Appendix A).
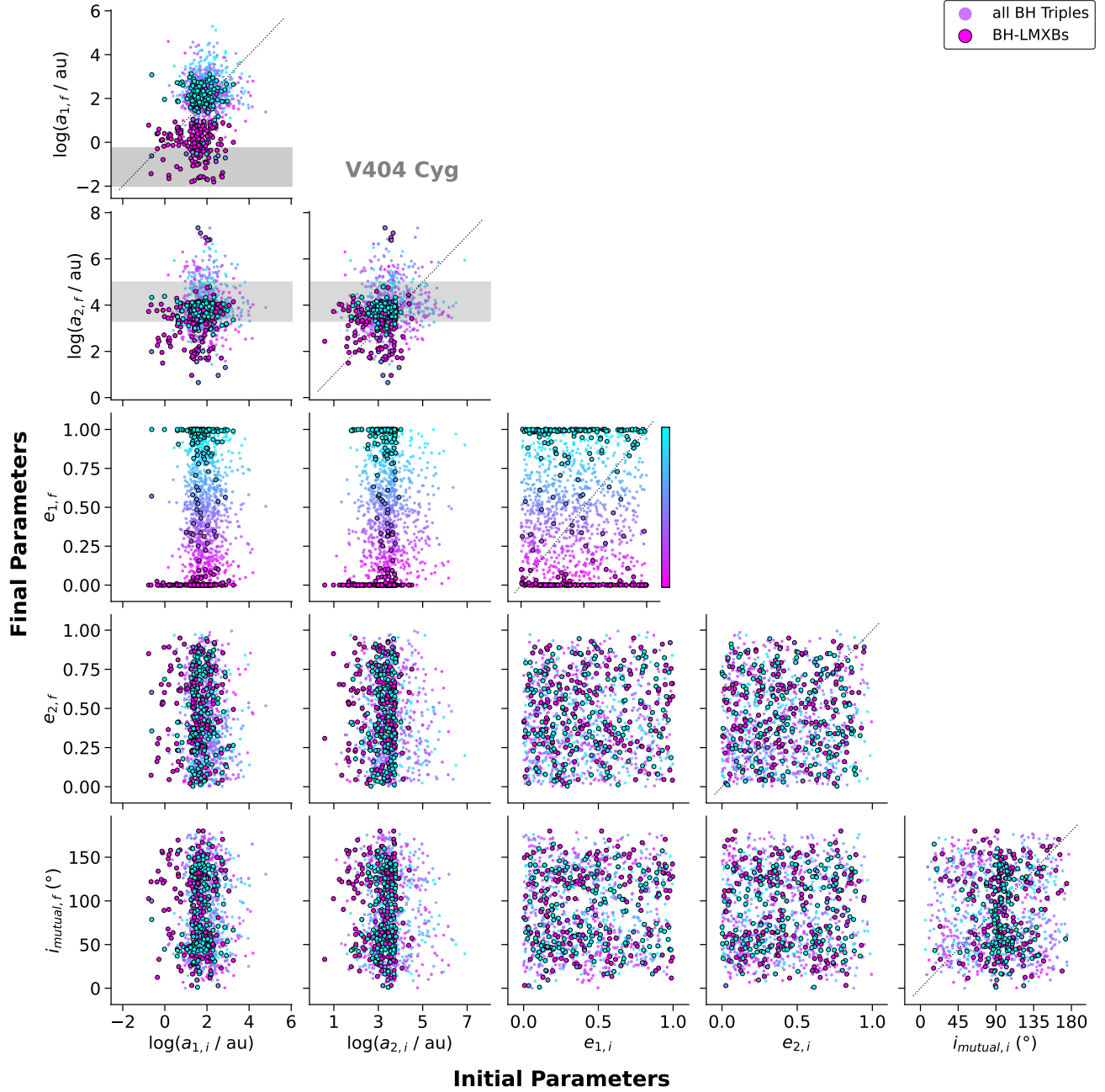
Figure 9. Corner plot comparing the initial (subscript 'i')to the final orbital parameters (subscript 'f'). We plot the distributions for the initial/final inner semi-major axis (a_1), outer semi-major axis (a_2), inner eccentricity (e_1), outer eccentricity (e_2), and mutual inclination (i_{mutual}). We show all of the triples with a BH primary in the inner binary and highlight those that become BH-LMXBs in black. The color of each point corresponds to the final e_1. In the diagonal plots, we show the 1 : 1 line.)
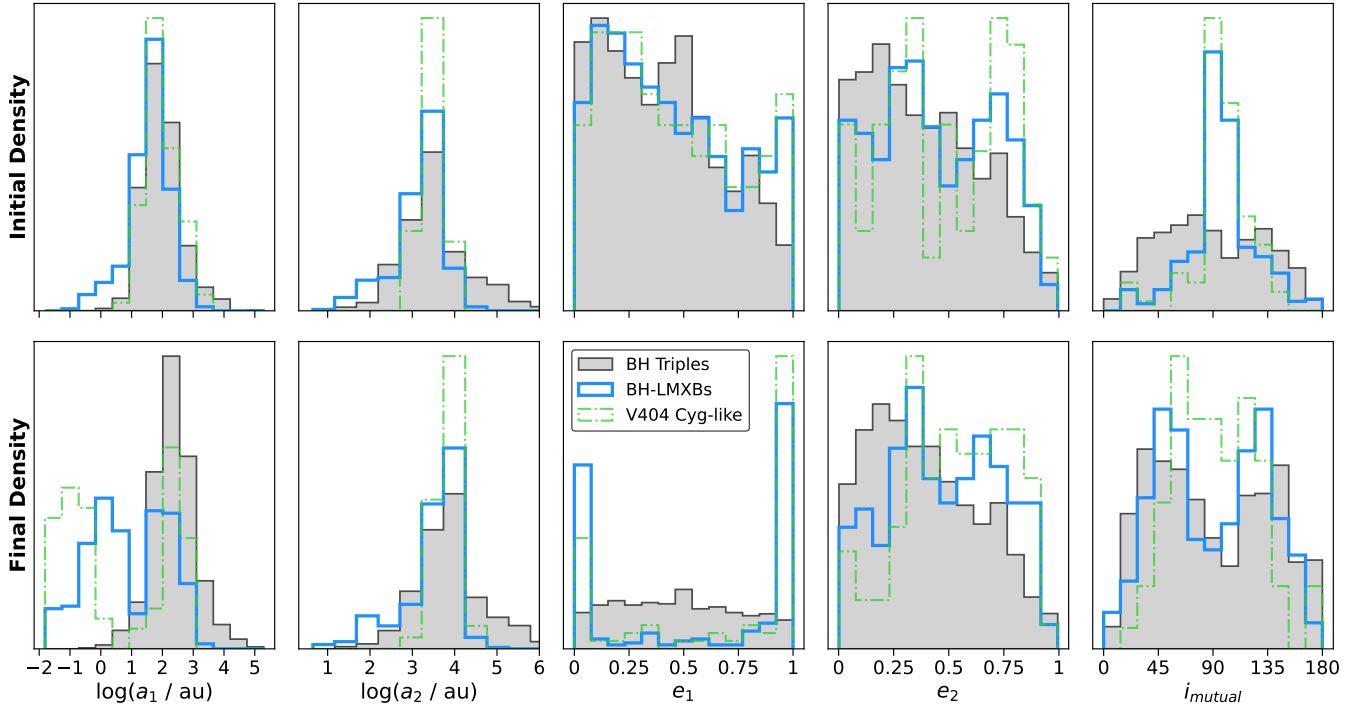
Figure 10. Histograms of initial (top) and final (bottom) probability density distributions of triples with a black hole in the inner binary. We include the triples that have detached inner binaries (gray), BH-LMXB inner binaries (blue), and BH-LMXB inner binaries with similar orbits to V404 Cygni (green dashed). All of the systems here did not experience a early mass transfer before BH formation. The parameters here are identical to those in Figure 9.

REFERENCES

Andrews, J. J., & Kalogera, V. 2022, ApJ, 930, 159,
doi: 10.3847/1538-4357/ac66d6

Angelo, I., Naoz, S., Petigura, E., et al. 2022, AJ, 163, 227,
doi: 10.3847/1538-3881/ac6094

Antonini, F., Chatterjee, S., Rodriguez, C. L., et al. 2016,
ApJ, 816, 65, doi: 10.3847/0004-637X/816/2/65

Arnason, R. M., Papei, H., Barmby, P., Bahramian, A., &
Gorski, M. D. 2021, MNRAS, 502, 5455,
doi: 10.1093/mnras/stab345

Arzoumanian, Z., Chernoff, D. F., & Cordes, J. M. 2002,
ApJ, 568, 289, doi: 10.1086/338805

Atri, P., Miller-Jones, J. C. A., Bahramian, A., et al. 2019,
MNRAS, 489, 3116, doi: 10.1093/mnras/stz2335

Bahramian, A., & Degenaar, N. 2023, in Handbook of
X-ray and Gamma-ray Astrophysics, 120,
doi: 10.1007/978-981-16-4544-0_94-1

Bataille, M., Libert, A. S., & Correia, A. C. M. 2018,
MNRAS, 479, 4749, doi: 10.1093/mnras/sty1758

Beer, M. E., & Podsiadlowski, P. 2002, MNRAS, 331, 351,
doi: 10.1046/j.1365-8711.2002.05189.x

Bhaskar, H., Li, G., Hadden, S., Payne, M. J., & Holman,
M. J. 2021, AJ, 161, 48, doi: 10.3847/1538-3881/abcbfc

Burdge, K. B., El-Badry, K., Kara, E., et al. 2024, arXiv
e-prints, arXiv:2404.03719,
doi: 10.48550/arXiv.2404.03719

Chen, X., Zhang, S. N., & Ding, G. Q. 2006, ApJ, 650, 299,
doi: 10.1086/506338

Chou, Y., & Grindlay, J. E. 2001, ApJ, 563, 934,
doi: 10.1086/324038

Clark, D. H., & Parkinson, J. H. 1975, Nature, 258, 408,
doi: 10.1038/258408a0

Corbet, R. H. D., Asai, K., Dotani, T., & Nagase, F. 1994,
ApJL, 436, L15, doi: 10.1086/187622

Cordes, J. M., & Chernoff, D. F. 1998, ApJ, 505, 315,
doi: 10.1086/306138

Corral-Santana, J. M., Casares, J., Muñoz-Darias, T., et al.
2016, A&A, 587, A61, doi: 10.1051/0004-6361/201527130

Dage, K. C., Bahramian, A., Naoz, S., et al. 2024, MNRAS,
529, 1347, doi: 10.1093/mnras/stae578

Dashwood Brown, C., Gandhi, P., & Zhao, Y. 2024,
MNRAS, 527, L82, doi: 10.1093/mnrasl/slad151

Dosopoulou, F., & Kalogera, V. 2016, ApJ, 825, 71, doi: 10.3847/0004-637X/825/1/71

Duchêne, G., Bouvier, J., Moraux, E., et al. 2013, A&A, 555, A137, doi: 10.1051/0004-6361/201321691

Duquennoy, A., & Mayor, M. 1991, A&A, 248, 485

Eggleton, P. P. 1983, ApJ, 268, 368, doi: 10.1086/160960

Eggleton, P. P., Kiseleva, L. G., & Hut, P. 1998, ApJ, 499, 853, doi: 10.1086/305670

Eggleton, P. P., & Kiseleva-Eggleton, L. 2001, ApJ, 562, 1012, doi: 10.1086/323843

Eggleton, P. P., & Verbunt, F. 1986, MNRAS, 220, 13P, doi: 10.1093/mnras/220.1.13P

El-Badry, K., & Rix, H.-W. 2018, Monthly Notices of the Royal Astronomical Society, 480, 4884, doi: 10.1093/mnras/sty2186

El-Badry, K., Rix, H.-W., & Weisz, D. R. 2018, ApJL, 860, L17, doi: 10.3847/2041-8213/aaca9c

El-Badry, K., Rix, H.-W., Quataert, E., et al. 2023a, MNRAS, 518, 1057, doi: 10.1093/mnras/stac3140

El-Badry, K., Rix, H.-W., Cendes, Y., et al. 2023b, MNRAS, 521, 4323, doi: 10.1093/mnras/stad799

El-Badry, K., Simon, J. D., Reggiani, H., et al. 2024a, The Open Journal of Astrophysics, 7, 27, doi: 10.33232/001c.116675

El-Badry, K., Rix, H.-W., Latham, D. W., et al. 2024b, arXiv e-prints, arXiv:2405.00089, doi: 10.48550/arXiv.2405.00089

Fabian, A. C., Pringle, J. E., & Rees, M. J. 1975, MNRAS, 172, 15, doi: 10.1093/mnras/172.1.15P

Fabrycky, D., & Tremaine, S. 2007, ApJ, 669, 1298, doi: 10.1086/521702

Fragile, P. C., & Anninos, P. 2005, ApJ, 623, 347, doi: 10.1086/428433

Fragile, P. C., Blaes, O. M., Anninos, P., & Salmonson, J. D. 2007, ApJ, 668, 417, doi: 10.1086/521092

Fragione, G., Capuzzo-Dolcetta, R., & Kroupa, P. 2017, MNRAS, 467, 451, doi: 10.1093/mnras/stx106

Fragione, G., Grishin, E., Leigh, N. W. C., Perets, H. B., & Perna, R. 2019, MNRAS, 488, 47, doi: 10.1093/mnras/stz1651

Fragione, G., & Loeb, A. 2017, NewA, 55, 32, doi: 10.1016/j.newast.2017.03.002

Fragione, G., Loeb, A., & Rasio, F. A. 2020, ApJL, 902, L26, doi: 10.3847/2041-8213/abbc0a

Fragos, T., Lehmer, B. D., Naoz, S., Zezas, A., & Basu-Zych, A. 2013a, ApJL, 776, L31, doi: 10.1088/2041-8205/776/2/L31

Fragos, T., Willems, B., Kalogera, V., et al. 2009, ApJ, 697, 1057, doi: 10.1088/0004-637X/697/2/1057

Fragos, T., Lehmer, B., Tremmel, M., et al. 2013b, ApJ, 764, 41, doi: 10.1088/0004-637X/764/1/41

Fragos, T., Andrews, J. J., Bavera, S. S., et al. 2023, ApJS, 264, 45, doi: 10.3847/1538-4365/ac90c1

Fryer, C. L., Belczynski, K., Wiktorowicz, G., et al. 2012, ApJ, 749, 91, doi: 10.1088/0004-637X/749/1/91

Fryer, C. L., Woosley, S. E., & Hartmann, D. H. 1999, ApJ, 526, 152, doi: 10.1086/307992

Giesler, M., Clausen, D., & Ott, C. D. 2018, MNRAS, 477, 1853, doi: 10.1093/mnras/sty659

Grimm, H. J., Gilfanov, M., & Sunyaev, R. 2002, A&A, 391, 923, doi: 10.1051/0004-6361:20020826

Grindlay, J. E., Bailyn, C. D., Cohn, H., et al. 1988, ApJL, 334, L25, doi: 10.1086/185305

Grishin, E., & Perets, H. B. 2022, MNRAS, 512, 4993, doi: 10.1093/mnras/stac706

Grishin, E., Perets, H. B., Zenati, Y., & Michaely, E. 2017, MNRAS, 466, 276, doi: 10.1093/mnras/stw3096

Hamers, A., Bar-Or, B., Petrovich, C., & Antonini, F. 2018, The Astrophysical Journal, 865, 2, doi: 10.3847/1538-4357/aadae2

Hamers, A. S., & Thompson, T. A. 2019, ApJ, 882, 24, doi: 10.3847/1538-4357/ab321f

Hansen, B. M. S., & Phinney, E. S. 1997, MNRAS, 291, 569, doi: 10.1093/mnras/291.3.569

Hills, J. G. 1976, MNRAS, 175, 1P, doi: 10.1093/mnras/175.1.1P

Hoang, B.-M., Naoz, S., & Sloneker, M. 2022, ApJ, 934, 54, doi: 10.3847/1538-4357/ac7787

Hobbs, G., Faulkner, A., Stairs, I. H., et al. 2004, MNRAS, 352, 1439, doi: 10.1111/j.1365-2966.2004.08042.x

Hurley, J. R., Pols, O. R., & Tout, C. A. 2000, MNRAS, 315, 543, doi: 10.1046/j.1365-8711.2000.03426.x

Hurley, J. R., Tout, C. A., & Pols, O. R. 2002, Monthly Notices of the Royal Astronomical Society, 329, 897, doi: 10.1046/j.1365-8711.2002.05038.x

Hurley, J. R., Tout, C. A., & Pols, O. R. 2002, MNRAS, 329, 897, doi: 10.1046/j.1365-8711.2002.05038.x

Hut, P. 1980, A&A, 92, 167

Ivanova, N. 2011, ApJ, 730, 76, doi: 10.1088/0004-637X/730/2/76

Ivanova, N., Justham, S., & Podsiadlowski, P. 2015, MNRAS, 447, 2181, doi: 10.1093/mnras/stu2582

Ivanova, N., Justham, S., & Ricker, P. 2020, Common Envelope Evolution, doi: 10.1088/2514-3433/abb6f0

Ivanova, N., Podsiadlowski, P., & Spruit, H. 2002, MNRAS, 334, 819, doi: 10.1046/j.1365-8711.2002.05543.x

Ivanova, N., Justham, S., Chen, X., et al. 2013, A&A Rv, 21, 59, doi: 10.1007/s00159-013-0059-2

Jermyn, A. S., Bauer, E. B., Schwab, J., et al. 2023, ApJS, 265, 15, doi: 10.3847/1538-4365/acae8d

Jonker, P. G., & Nelemans, G. 2004, MNRAS, 354, 355, doi: 10.1111/j.1365-2966.2004.08193.x

Jurado, C., Naoz, S., Lam, C. Y., & Hoang, B.-M. 2024, ApJ, 971, 95, doi: 10.3847/1538-4357/ad55ee

Justham, S., Rappaport, S., & Podsiadlowski, P. 2006, MNRAS, 366, 1415, doi: 10.1111/j.1365-2966.2005.09907.x

Kaib, N. A., & Raymond, S. N. 2014, ApJ, 782, 60, doi: 10.1088/0004-637X/782/2/60

Kalogera, V. 1996, ApJ, 471, 352, doi: 10.1086/177974

—. 1999a, ApJ, 521, 723, doi: 10.1086/307562

—. 1999b, ApJ, 521, 723, doi: 10.1086/307562

—. 2000, ApJ, 541, 319, doi: 10.1086/309400

Kalogera, V., & Webbink, R. F. 1996, ApJ, 458, 301, doi: 10.1086/176813

—. 1998, ApJ, 493, 351, doi: 10.1086/305085

Kaspi, V. M., Bailes, M., Manchester, R. N., Stappers, B. W., & Bell, J. F. 1996, Nature, 381, 584, doi: 10.1038/381584a0

Khargharia, J., Froning, C. S., & Robinson, E. L. 2010, ApJ, 716, 1105, doi: 10.1088/0004-637X/716/2/1105

Kimball, C., Imperato, S., Kalogera, V., et al. 2023, ApJL, 952, L34, doi: 10.3847/2041-8213/ace526

King, A., & Nixon, C. 2016, MNRAS, 462, 464, doi: 10.1093/mnras/stw1598

Kiseleva, L. G., Eggleton, P. P., & Mikkola, S. 1998, MNRAS, 300, 292, doi: 10.1046/j.1365-8711.1998.01903.x

Kobulnicky, H. A., Kiminki, D. C., Lundquist, M. J., et al. 2014, ApJS, 213, 34, doi: 10.1088/0067-0049/213/2/34

Kozai, Y. 1962, AJ, 67, 591, doi: 10.1086/108790

Kremer, K., Chatterjee, S., Rodriguez, C. L., & Rasio, F. A. 2018, ApJ, 852, 29, doi: 10.3847/1538-4357/aa99df

Kremer, K., Lu, W., Rodriguez, C. L., Lachat, M., & Rasio, F. A. 2019, ApJ, 881, 75, doi: 10.3847/1538-4357/ab2e0c

Kroupa, P. 2001, MNRAS, 322, 231, doi: 10.1046/j.1365-8711.2001.04022.x

Kuntz, A. 2022, PhRvD, 105, 024017, doi: 10.1103/PhysRevD.105.024017

Lai, D., Bildsten, L., & Kaspi, V. M. 1995, ApJ, 452, 819, doi: 10.1086/176350

Lehmer, B. D., Berkeley, M., Zezas, A., et al. 2014, ApJ, 789, 52, doi: 10.1088/0004-637X/789/1/52

Lense, J., & Thirring, H. 1918, Physikalische Zeitschrift, 19, 156

Levesque, E. M., Massey, P., Olsen, K. A. G., et al. 2005, ApJ, 628, 973, doi: 10.1086/430901

Lidov, M. L. 1962, Planet. Space Sci., 9, 719, doi: 10.1016/0032-0633(62)90129-0

Lim, H., & Rodriguez, C. L. 2020, PhRvD, 102, 064033, doi: 10.1103/PhysRevD.102.064033

Liu, B., & Lai, D. 2017, ApJL, 846, L11, doi: 10.3847/2041-8213/aa8727

Liu, B., Muñoz, D. J., & Lai, D. 2015, MNRAS, 447, 747, doi: 10.1093/mnras/stu2396

Lorimer, D. R., Bailes, M., & Harrison, P. A. 1997, MNRAS, 289, 592, doi: 10.1093/mnras/289.3.592

Lu, C. X., & Naoz, S. 2019, MNRAS, 484, 1506, doi: 10.1093/mnras/stz036

Lyne, A. G., & Lorimer, D. R. 1994, Nature, 369, 127, doi: 10.1038/369127a0

Maccarone, T. J. 2002, MNRAS, 336, 1371, doi: 10.1046/j.1365-8711.2002.05876.x

Mandel, I. 2016, MNRAS, 456, 578, doi: 10.1093/mnras/stv2733

Mardling, R. A., & Aarseth, S. J. 2001, MNRAS, 321, 398, doi: 10.1046/j.1365-8711.2001.03974.x

Martin, R. G., Tout, C. A., & Pringle, J. E. 2008, MNRAS, 387, 188, doi: 10.1111/j.1365-2966.2008.13148.x

Mata Sanchez, D., Torres, M. A. P., Casares, J., et al. 2024, arXiv e-prints, arXiv:2408.13310, doi: 10.48550/arXiv.2408.13310

Michaely, E., & Perets, H. B. 2014, ApJ, 794, 122, doi: 10.1088/0004-637X/794/2/122

—. 2016, MNRAS, 458, 4188, doi: 10.1093/mnras/stw368

—. 2020, MNRAS, 498, 4924, doi: 10.1093/mnras/staa2720

Miller-Jones, J. C. A., Jonker, P. G., Nelemans, G., et al. 2009, MNRAS, 394, 1440, doi: 10.1111/j.1365-2966.2009.14404.x

Miller-Jones, J. C. A., Tetarenko, A. J., Sivakoff, G. R., et al. 2019, Nature, 569, 374, doi: 10.1038/s41586-019-1152-0

Mirabel, I. F. 2017, in IAU Symposium, Vol. 324, New Frontiers in Black Hole Astrophysics, ed. A. Gomboc, 303–306, doi: 10.1017/S1743921316012904

Mirabel, I. F., Dhawan, V., Mignani, R. P., Rodrigues, I., & Guglielmetti, F. 2001, Nature, 413, 139, doi: 10.1038/35093060

Mirabel, I. F., & Rodrigues, I. 2003, Science, 300, 1119, doi: 10.1126/science.1083451

Moe, M., & Di Stefano, R. 2017, ApJS, 230, 15, doi: 10.3847/1538-4365/aa6fb6

Morningstar, W. R., Miller, J. M., Reis, R. C., & Ebisawa, K. 2014, ApJL, 784, L18, doi: 10.1088/2041-8205/784/2/L18

Motta, S. E., Kajava, J. J. E., Sánchez-Fernández, C., et al. 2017, MNRAS, 471, 1797, doi: 10.1093/mnras/stx1699

Mushkin, J., & Katz, B. 2020, MNRAS, 498, 665, doi: 10.1093/mnras/staa2492

Naoz, S. 2016, ARA&A, 54, 441,
doi: 10.1146/annurev-astro-081915-023315

Naoz, S., & Fabrycky, D. C. 2014, ApJ, 793, 137,
doi: 10.1088/0004-637X/793/2/137

Naoz, S., Farr, W. M., Lithwick, Y., Rasio, F. A., &
Teyssandier, J. 2011, Nature, 473, 187,
doi: 10.1038/nature10076

—. 2013a, MNRAS, 431, 2155, doi: 10.1093/mnras/stt302

Naoz, S., Fragos, T., Geller, A., Stephan, A. P., & Rasio,
F. A. 2016, ApJL, 822, L24,
doi: 10.3847/2041-8205/822/2/L24

Naoz, S., Kocsis, B., Loeb, A., & Yunes, N. 2013b, ApJ,
773, 187, doi: 10.1088/0004-637X/773/2/187

Offner, S. S. R., Moe, M., Kratter, K. M., et al. 2023, in
Astronomical Society of the Pacific Conference Series,
Vol. 534, Protostars and Planets VII, ed. S. Inutsuka,
Y. Aikawa, T. Muto, K. Tomida, & M. Tamura, 275,
doi: 10.48550/arXiv.2203.10066

Paczyński, B. 1967, AcA, 17, 287

Patton, R. A., & Sukhbold, T. 2020, MNRAS, 499, 2803,
doi: 10.1093/mnras/staa3029

Paxton, B., Bildsten, L., Dotter, A., et al. 2011, ApJS, 192,
3, doi: 10.1088/0067-0049/192/1/3

Paxton, B., Cantiello, M., Arras, P., et al. 2013, ApJS, 208,
4, doi: 10.1088/0067-0049/208/1/4

Paxton, B., Marchant, P., Schwab, J., et al. 2015, ApJS,
220, 15, doi: 10.1088/0067-0049/220/1/15

Paxton, B., Schwab, J., Bauer, E. B., et al. 2018, ApJS,
234, 34, doi: 10.3847/1538-4365/aaa5a8

Paxton, B., Smolec, R., Schwab, J., et al. 2019, ApJS, 243,
10, doi: 10.3847/1538-4365/ab2241

Perets, H. B., & Kratter, K. M. 2012, ApJ, 760, 99,
doi: 10.1088/0004-637X/760/2/99

Perets, H. B., Li, Z., Lombardi, James C., J., & Milcarek,
Stephen R., J. 2016, ApJ, 823, 113,
doi: 10.3847/0004-637X/823/2/113

Podsiadlowski, P., Cannon, R. C., & Rees, M. J. 1995,
MNRAS, 274, 485, doi: 10.1093/mnras/274.2.485

Podsiadlowski, P., Ivanova, N., Justham, S., & Rappaport,
S. 2010, MNRAS, 406, 840,
doi: 10.1111/j.1365-2966.2010.16751.x

Podsiadlowski, P., & Rappaport, S. 2000, ApJ, 529, 946,
doi: 10.1086/308323

Podsiadlowski, P., Rappaport, S., & Han, Z. 2003,
MNRAS, 341, 385, doi: 10.1046/j.1365-8711.2003.06464.x

Portegies Zwart, S. F., Verbunt, F., & Ergma, E. 1997,
A&A, 321, 207, doi: 10.48550/arXiv.astro-ph/9701037

Poutanen, J., Veledina, A., Berdyugin, A. V., et al. 2022,
Science, 375, 874, doi: 10.1126/science.abl4679

Poveda, A., Ruiz, J., & Allen, C. 1967, Boletin de los
Observatorios Tonantzintla y Tacubaya, 4, 86

Prodan, S., & Murray, N. 2015, ApJ, 798, 117,
doi: 10.1088/0004-637X/798/2/117

Rappaport, S., Verbunt, F., & Joss, P. C. 1983, ApJ, 275,
713, doi: 10.1086/161569

Reid, M. J., McClintock, J. E., Steiner, J. F., et al. 2014,
ApJ, 796, 2, doi: 10.1088/0004-637X/796/1/2

Repetto, S., Davies, M. B., & Sigurdsson, S. 2012, MNRAS,
425, 2799, doi: 10.1111/j.1365-2966.2012.21549.x

Repetto, S., Igoshev, A. P., & Nelemans, G. 2017, MNRAS,
467, 298, doi: 10.1093/mnras/stx027

Repetto, S., & Nelemans, G. 2015, MNRAS, 453, 3341,
doi: 10.1093/mnras/stv1753

Rocha, K. A., Kalogera, V., Doctor, Z., et al. 2024, ApJ,
971, 133, doi: 10.3847/1538-4357/ad5955

Rodriguez, C. L., Morscher, M., Pattabiraman, B., et al.
2015, PhRvL, 115, 051101,
doi: 10.1103/PhysRevLett.115.051101

Romagnolo, A., Belczynski, K., Klencki, J., et al. 2023,
MNRAS, 525, 706, doi: 10.1093/mnras/stad2366

Romani, R. W. 1998, A&A, 333, 583

Rose, S. C., Naoz, S., & Geller, A. M. 2019, MNRAS, 488,
2480, doi: 10.1093/mnras/stz1846

Salas, J. M., Naoz, S., Morris, M. R., & Stephan, A. P.
2019, MNRAS, 487, 3029, doi: 10.1093/mnras/stz1515

Sana, H., de Mink, S. E., de Koter, A., et al. 2012, Science,
337, 444, doi: 10.1126/science.1223344

Sana, H., Le Bouquin, J. B., Lacour, S., et al. 2014, ApJS,
215, 15, doi: 10.1088/0067-0049/215/1/15

Sepinsky, J. F., Willems, B., Kalogera, V., & Rasio, F. A.
2007, ApJ, 667, 1170, doi: 10.1086/520911

Shahbaz, T., Ringwald, F. A., Bunn, J. C., et al. 1994,
MNRAS, 271, L10, doi: 10.1093/mnras/271.1.L10

Shakura, N. I. 1973, Soviet Ast., 16, 756

Shappee, B. J., & Thompson, T. A. 2013, ApJ, 766, 64,
doi: 10.1088/0004-637X/766/1/64

Shariat, C., Naoz, S., El-Badry, K., et al. 2024, arXiv
e-prints, arXiv:2407.06257,
doi: 10.48550/arXiv.2407.06257

Shariat, C., Naoz, S., Hansen, B. M. S., et al. 2023, ApJL,
955, L14, doi: 10.3847/2041-8213/acf76b

Shenar, T., Sana, H., Mahy, L., et al. 2022, Nature
Astronomy, 6, 1085, doi: 10.1038/s41550-022-01730-y

Steiner, J. F., Reis, R. C., Fabian, A. C., et al. 2012,
MNRAS, 427, 2552,
doi: 10.1111/j.1365-2966.2012.22128.x

Stephan, A. P., Martin, D. V., Naoz, S., Hughes, N. R., &
Shariat, C. 2024, arXiv e-prints, arXiv:2408.13307,
doi: 10.48550/arXiv.2408.13307

Stephan, A. P., Naoz, S., & Gaudi, B. S. 2018, AJ, 156, 128, doi: 10.3847/1538-3881/aad6e5

—. 2021, ApJ, 922, 4, doi: 10.3847/1538-4357/ac22a9

Stephan, A. P., Naoz, S., Ghez, A. M., et al. 2016, MNRAS, 460, 3494, doi: 10.1093/mnras/stw1220

Stephan, A. P., Naoz, S., Ghez, A. M., et al. 2019, in AAS/Division of Dynamical Astronomy Meeting, Vol. 51, AAS/Division of Dynamical Astronomy Meeting, 202.02

Su, Y., Lai, D., & Liu, B. 2021, PhRvD, 103, 063040, doi: 10.1103/PhysRevD.103.063040

Sukhbold, T., Ertl, T., Woosley, S. E., Brown, J. M., & Janka, H. T. 2016, ApJ, 821, 38, doi: 10.3847/0004-637X/821/1/38

Taam, R. E., & Ricker, P. M. 2010, NewAR, 54, 65, doi: 10.1016/j.newar.2010.09.027

Tauris, T. M., & van den Heuvel, E. P. J. 2006a, in Compact stellar X-ray sources, ed. W. H. G. Lewin & M. van der Klis, Vol. 39, 623–665, doi: 10.48550/arXiv.astro-ph/0303456

—. 2006b, in Compact stellar X-ray sources, ed. W. H. G. Lewin & M. van der Klis, Vol. 39, 623–665, doi: 10.48550/arXiv.astro-ph/0303456

Tavani, M. 1991, Nature, 351, 39, doi: 10.1038/351039a0

Tetarenko, B. E., Sivakoff, G. R., Heinke, C. O., & Gladstone, J. C. 2016, ApJS, 222, 15, doi: 10.3847/0067-0049/222/2/15

Thorsett, S. E., Arzoumanian, Z., Camilo, F., & Lyne, A. G. 1999, ApJ, 523, 763, doi: 10.1086/307771

Toonen, S., Boekholt, T. C. N., & Portegies Zwart, S. 2022, A&A, 661, A61, doi: 10.1051/0004-6361/202141991

Toonen, S., Hamers, A., & Portegies Zwart, S. 2016, Computational Astrophysics and Cosmology, 3, 6, doi: 10.1186/s40668-016-0019-0

Toonen, S., Perets, H. B., & Hamers, A. S. 2018, A&A, 610, A22, doi: 10.1051/0004-6361/201731874

Toonen, S., Portegies Zwart, S., Hamers, A. S., & Bandopadhyay, D. 2020, A&A, 640, A16, doi: 10.1051/0004-6361/201936835

van Paradijs, J., & White, N. 1995, ApJL, 447, L33, doi: 10.1086/309558

Verbunt, F., & Zwaan, C. 1981, A&A, 100, L7

Vigna-Gómez, A., Willcox, R., Tamborra, I., et al. 2024, PhRvL, 132, 191403, doi: 10.1103/PhysRevLett.132.191403

Voss, R., & Gilfanov, M. 2007, A&A, 468, 49, doi: 10.1051/0004-6361:20066614

Wang, S., Zhao, X., Feng, F., et al. 2024, Nature Astronomy, doi: 10.1038/s41550-024-02359-9

Weldon, G. C., Naoz, S., & Hansen, B. M. S. 2024, arXiv e-prints, arXiv:2405.20377, doi: 10.48550/arXiv.2405.20377

White, N. E., & van Paradijs, J. 1996, ApJL, 473, L25, doi: 10.1086/310380

Willems, B., Henninger, M., Levin, T., et al. 2005, ApJ, 625, 324, doi: 10.1086/429557

Wong, T.-W., Valsecchi, F., Ansari, A., et al. 2014, ApJ, 790, 119, doi: 10.1088/0004-637X/790/2/119

Wong, T.-W., Valsecchi, F., Fragos, T., & Kalogera, V. 2012, ApJ, 747, 111, doi: 10.1088/0004-637X/747/2/111

Woosley, S. E., & Weaver, T. A. 1995, ApJS, 101, 181, doi: 10.1086/192237

Zahn, J. P. 1977, A&A, 57, 383

Zhang, E., Naoz, S., & Will, C. M. 2023, arXiv e-prints, arXiv:2301.08271, doi: 10.48550/arXiv.2301.08271

Zhang, Z., Gilfanov, M., & Bogdán, Á. 2012, A&A, 546, A36, doi: 10.1051/0004-6361/201219015

Zubovas, K., Wynn, G. A., & Gualandris, A. 2013, ApJ, 771, 118, doi: 10.1088/0004-637X/771/2/118